

## **Nanozyme-based electrochemical biosensors for disease biomarker detection**

### **Author**

Mahmudunnabi, Rabbee G, Farhana, Fatema Zerine, Kashaninejad, Navid, Firoz, Shakhawat H, Shim, Yoon-Bo, Shiddiky, Muhammad JA

### **Published**

2020

### **Journal Title**

Analyst

### **Version**

Accepted Manuscript (AM)

### **DOI**

<https://doi.org/10.1039/d0an00558d>

### **Copyright Statement**

© 2020 Royal Society of Chemistry. This is the author-manuscript version of this paper. Reproduced in accordance with the copyright policy of the publisher. Please refer to the journal website for access to the definitive, published version.

### **Downloaded from**

<http://hdl.handle.net/10072/395360>

### **Griffith Research Online**

<https://research-repository.griffith.edu.au>

# Nanozymes-based electrochemical biosensors for disease biomarker detection

Rabbee G. Mahmudunnabi,<sup>a,‡</sup> Fatema Zerine Farhana,<sup>b,‡</sup> Navid Kashaninejad,<sup>c</sup> Shakhawat H.

Firoz,<sup>\* b</sup> Yoon-Bo Shim,<sup>\*d</sup> and Muhammad J. A. Shiddiky<sup>\*c, e</sup>

<sup>a</sup> Department of Molecular Science Technology, Pusan National University, Busan 46241, South Korea

<sup>b</sup> Department of Chemistry, Bangladesh University of Engineering and Technology, Dhaka, Bangladesh

<sup>c</sup> Queensland Micro and nanotechnology Centre, Griffith University, Nathan Campus, QLD 4111, Australia

<sup>d</sup> Department of Chemistry & Institute of BioPhysio-Sensor Technology, Pusan National University, Busan 46241, South Korea

<sup>e</sup> School of Environment and Science, Griffith University, Nathan Campus, QLD 4111, Australia.

Emails: [m.shiddiky@griffith.edu.au](mailto:m.shiddiky@griffith.edu.au) (MJAS), [ybshim@pusan.ac.kr](mailto:ybshim@pusan.ac.kr) (YBS), and [shfiroz@chem.buet.ac.bd](mailto:shfiroz@chem.buet.ac.bd) (SHF)

<sup>‡</sup>Equal contributor and first-named authors

## **Abstract**

In recent years, a new group of nanomaterials named as nanozymes that exhibit enzyme-mimic catalytic activity, has emerged as a promising alternative to natural enzymes. Nanozymes can address some of the intrinsic limitations of natural enzymes such as high cost, low stability, difficulty in storage, and specific working conditions (i.e., narrow substrate, temperature and pH ranges). Thus, synthesis and applications of hybrid and stimuli-responsive advanced nanozymes could revolutionize the current practice in life sciences and biosensor applications. On the other hand, electrochemical biosensors have long been used as an efficient way for quantitative detection of analytes (biomarkers) of interest. As such, the use of nanozymes in electrochemical biosensor is particularly important to achieve low cost and stable biosensors for prognostics, diagnostics, and therapeutic monitoring of diseases. Herein, we summarize the recent advances in the synthesis and characterization of common nanozymes and their application in electrochemical biosensor development. After briefly overviewing the applications of nanozymes in non-electrochemical-based biomolecular sensing systems, we thoroughly discuss the state-of-the-art advances in nanozyme-based electrochemical biosensors, including genosensor, immunosensor, cytosensor and aptasensor. The applications of nanozymes in microfluidic-based assays are also discussed separately. We also highlight the challenges of nanozymes-based electrochemical biosensors and provide some possible strategies to address these limitations. Finally, future perspectives on the development of nanozymes-based electrochemical biosensors for disease biomarker detection are presented. We envisage that standardization of nanozyme and their fabrication process may bring a paradigm shift in biomolecular sensing by fabricating highly specific, multi-enzyme mimicking nanozymes for the highly sensitive, selective, and low-biofouling electrochemical biosensor.

## 1. Introduction

The term “nanozymes” was first introduced by Pasquato and co-workers in 2004 to describe the ribonuclease-like activity of triazacyclononane functionalized gold nanoparticles (NPs) in the transphosphorylation reaction.<sup>1</sup> The definition of nanozyme has been solidified as enzyme-mimicking nanomaterials after the demonstration of intrinsic peroxidase-like activities of magnetite (Fe<sub>3</sub>O<sub>4</sub>) NPs in 2007.<sup>2,3</sup> Since then, hundreds of nanomaterials have been reported with enzyme-mimicking properties along with diverse applications. Nanozymes have shown considerable advantages over natural enzymes due to their high and tunable catalytic activities, ease of modification, large surface area, low cost, and large-scale production. As such, nanozymes are widely regarded as direct alternatives to natural enzymes. Along with enzyme-mimic activities, optical, electrical, and magnetic properties of certain nanozymes are ideal for most analytical applications. These characteristics greatly facilitate the integration and automation of multiple processes such as separation and detection procedures of molecular targets with immensely high speed, leading to a decrease in the preparatory steps and required time.<sup>2,4,5</sup> **Figure 1** summarizes the unique features of nanozymes and their applications in electrochemical sensors.

Tremendous advancements in nanotechnology have contributed significantly to the unprecedented growth and applications of nanozymes. These synergistic advances have led to the development of high-performance and ultra-sensitive platforms, including colorimetric, fluorometric, chemiluminescent, surface-enhanced Raman scattering, and electrochemical biosensors.<sup>6</sup> The most common nanozymes used in these sensing systems include metal NPs (e.g., Au NPs,<sup>7-9</sup> Pt NPs,<sup>9-13</sup> Pd NPs<sup>9,14</sup>), metal oxide NPs (e.g., CeO<sub>2</sub> NPs, CuO NPs, BiFeO<sub>3</sub> NPs, CoFe<sub>2</sub>O<sub>4</sub> NPs), carbon-based nanomaterials (e.g., carbon nanotubes (CNTs), and graphene

oxide (GO)). In general, nanozymes can oxidize a variety of chromogenic substrates (e.g., 3,3',5,5'-tetramethylbenzidine (TMB), 2,2'-azino-bis(3-ethylbenzthiazoline-6-sulfonic acid) (ABTS), 3,3'-diaminobenzidine (DAB), and o-phenylenediamine dihydrochloride (OPD)) in the presence of hydrogen peroxide ( $H_2O_2$ ) and produce a distinguishable color. This concept has already been proved useful to detect not only  $H_2O_2$  but also other biologically relevant molecules like glucose or lactate when it becomes a part of cascade enzymatic reactions or tandem catalysis by a hybrid nanozyme.

A hybrid nanozyme can be made through assembling either glucose oxidase (GOx) or oxidase-like nanozymes on the surface of iron oxide nanozyme or with other peroxidase mimics.<sup>15-17</sup> In this assembly, oxidase activity is crucial as it provides peroxidase-like nanozyme with hydrogen peroxide to induce a color change or emit light in colorimetric or fluorescent sensors respectively. Integration of two or more nanozymes could improve the catalytic efficiency by enhancing the proximity effect, i.e., the first enzymatic reaction occurs in close (nanoscale) proximity to the second enzyme, thereby overcoming the limitation of diffusion-limited kinetics and intermediate instability.<sup>17,18</sup> However, reversible surface passivation of pristine noble metal nanozyme with single-stranded DNA (ssDNA) or aptamer is an excellent way to develop on/off colorimetric sensors.<sup>19-22</sup> Another intriguing strategy is the self-regulated colorimetric sensors that uses the nanozyme activity of nanoceria to detect acetylcholinesterase, nerve agents, drugs, and bioactive ions.<sup>23</sup> Several other sensitive colorimetric sensors based on the functional nanozymes have also been reported for the detection of biothiols and proteins,<sup>24</sup> point-of-care (POC) testing of cocaine,<sup>25</sup> and lateral flow immunochromatographic analysis of glycoprotein<sup>26</sup> and bacteria.<sup>27</sup>

In electrochemical biosensors, nanozymes can be used in two ways: (i) as an electrode material for biomarker sensing or (ii) as a tracing tag for signal amplification. As an electrode material, nanozymes have widely been used to fabricate the third and fourth generations of glucose sensors<sup>28</sup> as well as to detect cancer cells.<sup>29,30</sup> High surface area and high density capture sites of the nanozymes could allow enhanced loading of the electroactive species at their surfaces, resulting in improved electrochemical responses. For example, Wang *et al.* used peroxidase-mimicking graphene-supported ferric porphyrin as a tracing tag for signal amplification in detecting DNA.<sup>31</sup> High loading of porphyrin on both sides of graphene oxide (GO) offered at attomolar-order of sensitivity.

Wei *et al.* published a review on nanozymes in 2013.<sup>32</sup> Since then, numerous review articles have been published on the synthesis, functions, and applications of nanozymes. For instance, Sun *et al.*<sup>33</sup> reviewed carbon-based nanozymes and their applications for the detection of disease biomarkers. Singh *et al.*<sup>34</sup> reviewed the biosensing applications of cerium oxide-based nanozymes. Gao *et al.*<sup>17</sup> discussed the synthesis and applications of Fe<sub>3</sub>O<sub>4</sub> and Fe<sub>2</sub>O<sub>3</sub> NPs-based nanozymes. Biomedical applications of other nanostructured materials as nanozymes have also been covered extensively in the literature.<sup>5,35-42</sup> Very recently, Huang *et al.*<sup>4</sup> and Wu *et al.*<sup>2</sup> discussed the classifications and mechanisms of enzyme-like activities, regulation and control over their activities. They also reviewed the applications of nanozymes in the fields of biomedical and environmental sciences. A recent book has provided an comprehensive overview of materials used for nanozyme synthesis and characterization along with cutting-edge biomedical and environmental applications.<sup>43</sup> However, to the best of our knowledge, no review paper is currently available for nanozyme based electrochemical biosensors for the detection of disease biomarkers.

This review covers the classifications, synthesis methods, current state-of-the-art development of nanozymes-based electrochemical biosensors. We focus on the applications of nanozyme-based electrochemical biosensors for disease biomarker detection published mostly from 2015 onward. We also highlight the challenges associated with nanozymes-based electrochemical biosensors and provide the possible solutions and strategies to address these limitations.

## 2. Common nanozymes for electrochemical biosensors

Intense research and investigation have been conducted to reveal the nanozyme activities of various nanostructured materials. Until now, several nanomaterials have been reported to have catalytic activities similar to peroxidase, oxidase, catalase, and superoxide dismutase (SOD). Based on the reaction mechanism, nanozymes can be divided into two main families<sup>4</sup>: (i) oxidoreductase family and (ii) hydrolase family. Oxidoreductase nanozymes catalyze the oxidation reaction, where reductants and oxidants work as electron donors and acceptors, respectively. Over the past several years, graphene- and AuNPs-based nanozymes have been demonstrated to possess excellent peroxidase-like activity to catalyze the oxidation of many substrates, such as TMB and ABTS in the presence of H<sub>2</sub>O<sub>2</sub>.<sup>4</sup> It also has been shown that other metallic nanoparticles have oxidoreductase activities. For example, Tremel *et al.* reported that MoO<sub>3</sub> nanoparticles work as nanozymes for the oxidation of SO<sub>3</sub><sup>2-</sup> to SO<sub>4</sub><sup>2-</sup> under physiological condition.<sup>44</sup> On the other hand, hydrolase nanozymes catalyze the hydrolysis reaction by cleaving chemical bonds. In this process, a larger molecule dissociates into two smaller molecules. For instance, gold nanoparticles have widely been used as common hydrolase nanozymes to catalyze hydrolysis reactions.<sup>45–47</sup>

In terms of the free radical scavenging capability, nanozymes can also be categorized as (i) antioxidants and (ii) pro-oxidants.<sup>48</sup> In biological systems, pro-oxidant induces oxidative stress by producing free radicals. For example, the presence of transition metal can produce hydroxyl radical (HO<sup>•</sup>) by Fenton chemistry.<sup>49</sup> Therefore, certain peroxidase or oxidase involved in the reaction of free radical generation could be regarded as pro-oxidant.<sup>48</sup> On the contrary, antioxidant nanozymes clean up or scavenge free radical by using catalase- or SOD-like activities.<sup>48</sup> SOD-mimetic catalyzes the dismutation of superoxide anions into hydrogen peroxide, which in turn, can be converted to molecular oxygen and water through catalase-like nanozyme. On the other hand, peroxidase-like may convert hydrogen peroxide into a hydroxyl-free radical and oxidized, and produced colored product. Similar colored products may also be produced by oxidase-like nanozyme through direct oxidation of a chromogenic substrate. **Figure 2** summarizes the classification of nanozymes based on both the reaction mechanism and free radical generation/scavenging.

Among the oxidoreductase nanozymes, peroxidase- and oxidase-mimicking nanomaterials are mostly explored for electrochemical biosensors (**Table 1**). The common nanomaterials with peroxidase mimetics includes metal nanoparticles (AuNPs,<sup>50</sup> PdNPs<sup>51</sup>), metal oxides (Fe<sub>2</sub>O<sub>3</sub>,<sup>52,53</sup> Au-NPFe<sub>2</sub>O<sub>3</sub>NC,<sup>54,55</sup> Fe<sub>3</sub>O<sub>4</sub> MNP,<sup>56</sup> CeO<sub>2</sub>/NiO,<sup>57</sup> and CuO<sup>58</sup>), core-shell nanostructure(Au@Pt<sup>59</sup>), dendrite (dealloyed-AuNi@pTBA,<sup>60</sup> Cu–Co alloy dendrite<sup>61</sup>), carbon-based composite(GO-AuNP,<sup>62</sup> His@AuNCs/rGO,<sup>63</sup> PtNPs decorated CNT<sup>64</sup>), and metal-organic frameworks (MOFs). Unlike other nanomaterials, MOFs have drawn enormous interest as a new class of nanozymes due to their uniform cavities which are likely to provide biomimetic active centers and enzyme-like pseudo-substrate-binding pockets.<sup>65</sup>



### 3. Synthesis of common nanozymes used in electrochemical biosensors

The peroxidase-like activity of the nanozymes is mainly dependent on their surface area to volume ratio (i.e., density of the exposed active sites at the surface of the nanozymes) as well as their affinity towards the organic substrates such as TMB and ABTS.<sup>2</sup> The size,<sup>8,90</sup> shape,<sup>91</sup> morphology,<sup>92</sup> compositions, and surface modification groups<sup>93,94</sup> of the nanozymes can also influence their peroxidase-like activities. It is important to note that size, shape, composition and morphology of the nanostructured materials can be controlled by changing reaction parameters,<sup>95,96</sup> precursor amount and volume<sup>97,98</sup> and selecting appropriate synthetic methods<sup>3</sup>.

Due to the potential applications of nanozymes in electronics,<sup>99</sup> therapeutics, optics,<sup>100</sup> catalysis<sup>101</sup> and biosensing<sup>102</sup> applications, there has been a demand for the design and synthesis of nanozymes with high peroxidase-like activities. Over the past few years, many attempts have been made to synthesize nanozymes with well-controlled size, shape, spatial arrangement, and compositions. These methods can be divided into two main categories: top-down and bottom-up approaches. The top-down approach is the solid-state processing of macroscopic materials to nanophasic products. This approach includes mechanical milling, nanolithography, laser ablation, sputtering and thermal decomposition. However, the top-down approach is not suitable to make well-controlled size and shape and may produce many crystallographic defects in the nanostructure. On the contrary, the bottom-up method follows building up of nanostructures through atom-by-atom or cluster-by-cluster or molecule-by-molecule approach. It offers nanomaterials with uniform size, shape, fewer defects and homogeneous chemical compositions. The bottom-up approach mostly includes processes such as sol-gel, reverse micelle, chemical vapour deposition (CVD), pyrolysis, biosynthesis, microwave-assisted, and flow synthesis, and most of these processes refer to as wet chemical synthesis.<sup>103–105</sup> In the following sections, we

highlight the synthesis of metal oxide, metallic and carbon-based nanozymes with different size, shape and morphology using top-down and bottom-up approaches.

### **3.1 Synthesis of metal oxides nanozymes**

Thermal decomposition (also called thermolysis) is a process where chemical bonds of a compound are subjected to dissociation through thermal energy resulting in the formation of monodispersed nanoparticles in a single step. Usually, an organometallic precursor is heated in a high-boiling point organic solvent in the presence of a suitable surfactant, such as oleic acid, 1-octadecene, 1-tetradecene or oleylamine. As an early attempt to synthesize monodispersed iron oxide nanocrystals, Park *et al.* slowly heated iron–oleate complex in 1-octadecene at different temperatures. They observed that temperature dependence of nucleation and growth kinetics were instrumental in monodisperse nanocrystal formation. They also reported that metal oxide NPs (i.e., Fe<sub>2</sub>O<sub>3</sub>, CoO, MnO, FeO@Fe, and MnFe<sub>2</sub>O<sub>4</sub>) with different sizes could be synthesized by using organic solvents with high boiling points, namely 1-hexadecene and trioctylamine (i.e., these solvents have the boiling point of 274°C and 365°C respectively). The high yield (>95%) and large scale production (40g) are two characteristic features that have made this process as state-of-the-art for nanocrystal synthesis.<sup>104</sup> Another study also supported that high temperature synthesis leads to the increases of the nanoparticle size due to comparatively higher reactivity of the metal complex in the solvent.<sup>106</sup> However, the metal oxide NPs with nanozyme activity prepared by this method are usually smaller in size, crystalline and dispersed only in the organic solvent.

The sol-gel process for metal oxides synthesis is a wet chemistry based technique, which is accomplished at room temperature. This method is comparatively cheaper than other wet

chemical methods. In this method, a sol is a stable dispersion of colloidal particles or polymers in a solvent, and a gel consists of a three-dimensional continuous network, which encloses a liquid phase. The sol-gel method involves hydrolysis and condensation of metal alkoxides, leading to the dispersion of metal oxide particles in a sol, followed by drying or gelling through solvent removal or by using a chemical reaction. This method consists of several steps, namely hydrolysis, condensation, drying, and thermal treatment to realize the final product of metal oxide NPs.<sup>107–111</sup>

Solvothermal and hydrothermal synthesis methods are other well-established wet chemical methods to produce metal-oxide NPs. These methods are carried out in an autoclave or a Parr bomb at high temperature (100 to 1000°C) and high pressure (1 to 10000 bar). The main difference between hydrothermal and solvothermal methods is that water is used as a precursor solvent for hydrothermal synthesis, whereas organic solvents are used in solvothermal synthesis. These methods do not require a protective gas atmosphere and refluxing conditions and are more convenient compared to the coprecipitation and thermal decomposition methods. Metal oxide NPs obtain in these methods are highly pure, selective, reproducible and crystalline. Moreover, the crystalline characteristic of the NPs can be altered by total reaction time. For instance, it was reported that the transformation of hydrothermally produced iron oxide nanozymes from 0D to 3D structure is time-dependent.<sup>103</sup> Li *et al.* applied solvothermal reaction to synthesized metal-ion-doped (such as Sn<sup>4+</sup>, Fe<sup>3+</sup>, Co<sup>2+</sup>, and Ni<sup>2+</sup>) TiO<sub>2</sub> nanocomposites. The size and shape of the TiO<sub>2</sub>NPs were controlled by using lauryl alcohol both as solvent and surfactant for the reaction.<sup>112</sup>

Microwave-assisted chemical synthesis process is an alternative wet chemical technique for the synthesis of metal oxides NPs based nanozymes. Recent evidences suggest that this

method produced NPs with uniform-size and ultrafine-shape. In a conventional heating system, it is quite impossible to transfer the heat uniformly to the reactant precursor. In contrast, microwave-assisted synthesis provides uniform heating and thus reduces reaction time by increasing reaction kinetics. This method is safe, convenient and requires less energy for the completion of the reaction because of its fast nucleation and growth rate. Recently, several metal-oxide based nanozymes have been synthesized by using the microwave-assisted method. These include ZnO,<sup>113</sup>  $\alpha$ -Fe<sub>2</sub>O<sub>3</sub>,  $\beta$ -Fe<sub>2</sub>O<sub>3</sub>, Fe<sub>3</sub>O<sub>4</sub>,<sup>114</sup> CuO,<sup>115</sup> Cu<sub>2</sub>O,<sup>116</sup> Mn<sub>3</sub>O<sub>4</sub>, MnO<sub>2</sub>,<sup>117</sup> TiO<sub>2</sub>,<sup>118</sup> and Co<sub>3</sub>O<sub>4</sub>.<sup>119</sup> It is important to note that the phase and shape of the NPs can be altered by the properties of solvents used in the method. Guru *et al* have shown that the synthesis of iron oxide NPs by the microwave-assisted method could be drastically affected by using different glycols.<sup>120</sup> Three different glycols (ethylene glycol, polyethylene glycol and polypropylene glycol) with the same precursor under the same condition, resulted three NPs with different phases (Fe<sub>3</sub>O<sub>4</sub>,  $\alpha$ -Fe<sub>2</sub>O<sub>3</sub>, and  $\gamma$ -Fe<sub>2</sub>O<sub>3</sub>) and shapes (35, 29.9 and 28.2 nm).

### **3.2 Synthesis of metallic nanozymes**

Metallic NPs are synthesized by a range of physical processes, chemical reductions, and biological methods. The commonly used physical processes for the synthesis of metallic NPs include grinding, UV irradiation, microwave irradiation, and laser ablation methods. Chemical reduction is the most widely used techniques where metal salts are reduced in the presence of a suitable reducing agent.<sup>121-122</sup> Citrate has been used as a reducing agent for chloroauric acid and silver nitrate to synthesize AuNPs and AgNPs, respectively.<sup>123,124</sup> Metallic NPs produced by this method have the high tendency to aggregate. To stop this tendency, stabilizing agents, such as polyvinyl alcohol, poly (vinylpyrrolidone), bovine serum albumin (BSA), citrate and cellulose,

are mostly used in the reduction reactions. The size of the NPs can be tuned by changing the ratio of the stabilizing agent and the metal salt.<sup>125</sup> In biological methods, non-toxic and inexpensive microbes are used to produce a variety of metallic NPs with different size, shape and composition. In summary, biological methods are environmentally friendly, whereas chemical reduction methods are hazardous and physical process suffers from high energy input.

### **3.3 Synthesis of carbon-based nanozymes**

In this section, the synthesis of graphene oxide, CNTs, carbon nanodots based nanozymes are discussed. Graphene oxide (GO) is a nonconductive and hydrophilic carbon nanomaterial. In general, synthesis of GO from graphite is a two-step process.<sup>126,127</sup> In the first step, graphite flakes are oxidized to graphite oxide to have oxygen-containing functional groups (*e.g.*, epoxy (C–O–C), hydroxyl (OH), carbonyl (C=O) and carboxyl (R–COOH)) into the basal plane or edge of the graphene sheet. As a result of the oxygen-containing groups, the interlayer distance in GO expands and makes the atomic-thick layers hydrophilic as well. In the second step, oxidized layers can be subjected to the exfoliation under moderate sonication, resulting in releasing GO. In 1859, Brodie first synthesized GO by adding potassium chlorate to a slurry of graphite in the presence of fuming nitric acid.<sup>128</sup> This process needs 3 to 4 days to be completed. In 1898, Staudenmaier improved the Brodie's protocol by adding concentrated sulfuric acid and fuming nitric acid followed by the addition of chlorate in the reaction mixture. This method produces highly oxidized GO. However, these two processes suffer a long reaction time. Most widely used Hummer's method,<sup>129</sup> reported in 1958, avoids this disadvantage where high-quality GO can be produced within 2 h. In this method, graphite is oxidized with  $\text{KMnO}_4$  and  $\text{NaNO}_3$  in concentrated  $\text{H}_2\text{SO}_4$ . Notably, all three methods produce toxic gas(es):  $\text{ClO}_2(\text{g})$  and/or  $\text{NO}_x(\text{g})$ ,

the former one is explosive. Later, Tour improved the Hummer's method by replacing  $\text{NaNO}_3$  with the mixture of  $9\text{H}_2\text{SO}_4:\text{H}_3\text{PO}_4$ . The reaction mixture was fortified with the doubled amount of  $\text{KMnO}_4$  as compared to the Hummer's method. This method does not produce any toxic gas and generates oxidized GO with a more regular carbon framework and larger sheet size.<sup>126,130–132</sup> Over the past several years, GO has widely been used to synthesize different hybrid nanostructured materials to produce a range of GO-based nanozymes. For example, Ruan *et al.* synthesized GO/Fe-MOF nanozyme via mixing the negatively charged GO with the positively charged Fe-MOF. Electrostatic interactions between GO and Fe-MOF hold them together.<sup>133</sup> A similar phenomenon was used for the synthesis of GO-AuNP nanozymes. During the aging step of the synthesis, gold ion was adsorbed on the surface of the GO. This step was followed by a reduction reaction with sodium citrate, resulting in the formation of AuNPs onto the GO (i.e., GO-AuNP hybrid).<sup>62</sup>

There are various methods for the synthesis, purifications, dispersion, and functionalisation of CNTs.<sup>134</sup> These materials offers enormous benefits in real world applications. In particular, they are attractive for uses in bimolecular sensors for environmental and health monitoring.<sup>135</sup> Recent evidences suggest that CNT based materials possess excellent peroxidase-like activities.<sup>136</sup> Qu *et al* synthesised oxygenated-group-enriched carbon nanotubes (o-CNTs) via a one-pot oxidation reflux method.<sup>137</sup> The o-CNTs exhibited enhanced peroxidase-like activity for the catalytic reaction over a broad pH range. It was used to catalyse the formation of hydroxyl radical, killing bacteria efficiently and protecting the tissue against edema and inflammation induced by bacteria infections. Among other CNT based materials, single-walled carbon nanotubes (SWCNT) and multi-walled carbon nanotubes (MWCNT) have widely been used to fabricate metal nanoparticle ( $\text{Fe}_3\text{O}_4$ ,  $\text{ZnO}$ ) or GO based hybrid nanozymes.<sup>138–141</sup>

Compared with their single component, these hybrid materials offered enhanced peroxidase-like activities, presumably resulting from the synergetic effects of metallic nanoparticles or GO and conducting CNT (i.e., SWCNT or MWCNT). Recently, it has been shown that Fe<sub>3</sub>O<sub>4</sub> nanoparticles loaded on GO-dispersed CNTs offers stronger enzyme-like activity.<sup>140</sup> To synthesise this hybrid materials, amphiphilic GO nanosheets could be employed as “surfactant” to disperse CNTs to create stable GO-dispersed CNT supports in water for covalently loading cubic Fe<sub>3</sub>O<sub>4</sub> nanoparticles. Compared with original Fe<sub>3</sub>O<sub>4</sub> and CNT-loaded Fe<sub>3</sub>O<sub>4</sub> nanoparticles, the GO/CNT–Fe<sub>3</sub>O<sub>4</sub> particles offered enhanced peroxidase-like activities. Similarly, iron containing hemin assembled with SWCNT showed enhanced peroxidase-like activity.<sup>142</sup> Hemin could be assembled on the surface of SWCNT through non-covalent functionalization by  $\pi$ – $\pi$  stacking, and resulted much higher peroxidase-like activity than the activity of hemin alone.

Carbon nanodots (CD) or carbon quantum dots (CQD) are a novel class of carbon nanomaterials with size less than 10 nm but can be as small as 1 nm. These materials have commonly been synthesized by using top-down and bottom-up approaches.<sup>143-147</sup> Each approach has its own advantages and disadvantages. Top-down approaches are widely used for the synthesis of CD due to the adequate amount of raw material, scaled-up production and smooth operation. On the other hand, bottom-up approaches give attractive opportunities to control particle size, shape, and properties. Recently, green synthesis of CD has become more popular than the conventional hydrothermal, solvothermal, electrochemical, and electron-beam lithography methods that usually require toxic chemicals and a large amount of heat energy.<sup>144, 146, 147</sup> In green synthesis, the organic precursor is replaced by biomass materials and does not require external energy supply.<sup>147</sup> It has been shown that CD, CDQ, doped CD/graphene QDs, and CD/graphene QDs nanocomposites possess peroxidase-like activity.<sup>146</sup> The design, catalytic

process, property study, and bio sensing application of these materials have also been discussed in the literature.<sup>143-147</sup> These materials have been used in developing biomolecular sensors for the detection many biological and environmentally significant targets including glutathione,<sup>148</sup> glucose,<sup>149</sup> and mercury ions.<sup>150</sup>

#### **4. Nanozyme as a substitute of HRP**

The enzyme-linked immunosorbent assay (ELISA) is the most routinely used technique for detecting and quantifying peptides and antigens. In ELISA, an enzyme-linked primary antibody (direct ELISA) or secondary antibody (indirect or sandwich ELISA) specifically recognizes an antigen. Until now, HRP is the most widely used enzyme reporter in ELISA. It catalyzes the oxidation of TMB in the presence of H<sub>2</sub>O<sub>2</sub> to produce a colorimetric signal, and the intensity of the signal is proportional to the recognized antigen concentration. Despite having many advantages including high substrate turnover, small size, and facile conjugation ability with other biological receptors, HRP suffers several drawbacks. The major drawback associated with HRP is its low tolerance to many preservatives such as sodium azide that inactivates peroxidase activity even at low concentration. It also undergoes proteolytic degradation, and its enzymatic activity is limited to a narrow range of pH and temperature.<sup>5</sup> Moreover, conventional ELISA lacks sensitivity to detect ultra-low concentration of biomolecules, especially in the early stages of the diseases.<sup>151</sup> To overcome these limitations, numerous nanostructured material based nanozymes including MOFs based hybrid nanozymes (described above), have been developed, which are believed to be direct surrogates of HRP.<sup>42</sup> For instance, Ruan *et al.* reported the third generation of 2D GO/Fe-MOF hybrid nanozymes, named nanozyme nest, which was used in a conventional sandwich ELISA to detect benzo[a]pyrene-7,8-diol 9,10-epoxide–DNA adduct



(BPDE–DNA), a woodsmoke biomarker found in the blood.<sup>133</sup> This method showed enhanced sensitivity for the oxidation of TMB by dual peroxidase active nanozyme nest(Fe-MOF and GO). The value of Michaelis-Menten constant,  $K_m$ , (0.3599mM for nanozyme nest vs. 0.4072 mM for HRP) clearly revealed that nanozyme nest offers higher TMB affinity than that of HRP. Importantly, this hybrid nanozyme reports the lower LOD value in compared to that of the HRP, suggesting the better sensitivity of nanozyme nest over HRP in detecting biomolecules.<sup>133</sup>

The peroxidase-like activity of nanozyme can be increased via rational design of nanostructured materials as multifunctional nanozymes. Heteroatom doping and sequence of doping are two effective ways to increase the peroxidase-like activity and specificity of nanozymes. For instance, up to a 100-fold increase in catalytic activity has been reported for the nitrogen-doped (N-doped) reduced graphene oxide (N-rGO) nanozymes in compared to the reduced graphene oxide (rGO) alone.<sup>152</sup> Density functional theory (DFT) calculation revealed that N-rGO selectively activates  $H_2O_2$  over  $O_2$  and  $\bullet O_2^-$  and forms stable radical oxygen species adjacent to N-doped sites. These radical oxygen species, in turn, oxidize peroxidase substrates (e.g., TMB) and offer enhanced responses. In another study, Kim *et al.* showed 1000-fold higher catalytic efficacy ( $k_{cat}/K_m$ ) of N and B co-doped reduced graphene oxide (NB-rGO) compared to that of the rGO alone. The catalytic performance of this material is very similar to that of the natural HRP. They have also demonstrated that the sequence of doping of the heteroatoms in the nanostructure materials could significantly affect the catalytic efficacy ( $k_{cat}/K_m$ ) of nanozymes. For example, the catalytic activity of BN-rGO resulted in  $\sim 30\%$  lower  $k_{cat}$  compared to that of the NB-rGO.<sup>150</sup> High surface to volume ratio,  $\pi$ - $\pi$  and hydrophobic interactions assist NB-rGO to acquire stronger affinity towards substrates (e.g., TMB) than that of HRP. Due to this property, NB-rGO nanozymes were able to detect C-reactive protein (CRP), a reliable biomarker for

inflammation, tissue damage and cardiovascular disease, via the oxidation-dependent rapid color change of TMB within 3 minutes. In contrast, HRP-based ELISA needs at least 10 minutes. It also shows three-times lower LOD ( $\sim 5\text{ng/mL}$  of CRP) than that of HRP.<sup>150</sup>

## 5. Applications of nanozymes in non-electrochemical-based assays

### 5.1 Lateral-flow immunodetection

Lateral-flow immunostrip (i.e., nanozyme-strip), a paper-based biosensor, is considered as one of the excellent demonstrations for POC testing of biomolecular targets because of its operational simplicity, rapid analysis, naked-eye detection and low cost. Generally, lateral flow biosensors composed of a sample pad, a conjugate pad, a nitrocellulose membrane containing test and control lines, and an absorbent pad. Many nanozymes have been integrated into this form of the assay. For example, Duan *et al.* reported a  $\text{Fe}_3\text{O}_4$  magnetic nanoparticle (MNP) based immunochromatographic strip to detect glycoprotein of ebolavirus (EBOV).<sup>26</sup> In this assay, MNP conjugated detection antibody (anti-EBOV) recognizes EBOV, which in turn forms a sandwich complex with the capture antibody in the test line. After the formation of immunocomplex, oxidation of the peroxidase substrate develops color for visual observation, indicating the presence of EBOV. Pre-processing the sample with immunomagnetic separation offered an additional sensitivity to the EBOV analysis. Overall, this strip demonstrates 100-fold higher sensitivity over the standard colloidal AuNPs based strip with the LOD of  $1\text{ ng/mL}$  of glycoprotein ( $\approx 240\text{pfu/ml}$ ). This method requires less than half an hour<sup>26</sup> and it is sensitive enough to detect Ebola at onset of symptoms.

Recently, porous platinum core-shell nanocatalysts (PtNCs) based immunostrip has been developed to detect p24 HIV capsid protein, a reliable marker for HIV diagnosis (**Figure 3**). In

this assay, both target specific antibody-functionalised PtNCs and orthogonally biotinylated camelid antibody fragments (nanobody-biotin) are designed to recognize the distinct regions of target p24 protein.<sup>153</sup> In the presence of test sample (i.e., serum or plasma contacting p24 protein), p24 protein-bound PtNCs become biotinylated through complexation with the biotinylated nanobody fragments. At the polystreptavidin-coated test line, rapid high affinity biotin–streptavidin binding enables a target dependent deposition of biotinylated p24 protein-bound PtNCs complex. PtNCs bound at the test line catalyze the oxidation of 4-chloro-1-naphthol/3,3'-diaminobenzidine, tetrahydrochloride (CN/DAB) substrate in the presence of H<sub>2</sub>O<sub>2</sub> producing an insoluble black product which is clearly visible with the naked eye. This method allows the detection of acute-phase HIV in clinical human plasma samples in under 20 min.

## **5.2. Colorimetric sensor**

Colorimetric detection of an analyte has the advantage of providing a fast response (color change) to obtain visual observation (naked eye) and subsequent UV-visible quantification. An advantage of naked-eye detection is that it can be employed as a first-pass screening test for rapid diagnosis of diseases. Once positive results are obtained, UV-vis or other quantities measurements (i.e., electrochemical detection) could be performed to quantify the level and severity of diseases to determine the treatment options, management strategy, which could significantly reduce the cost and time associated with the disease diagnosis and management. This feature of colorimetric sensors makes it suitable for developing rapid and inexpensive screening tools in the fields of medicine (i.e., detection of disease-specific molecules, proteins, and cells), biotechnology, and environmental sciences. As peroxidase mimic nanozyme can

oxidise chromogenic substrates (e.g., TMB, ABTS, and OPD) and produce a color in the presence of H<sub>2</sub>O<sub>2</sub>, it can directly detect H<sub>2</sub>O<sub>2</sub> or other H<sub>2</sub>O<sub>2</sub> producing substrates (e.g., glucose).

Peroxidase-like activity of both the iron oxide nanocomposites (e.g., PDDA coated Fe<sub>3</sub>O<sub>4</sub> MNPs,<sup>154</sup> mesoporous silica encapsulated Fe<sub>3</sub>O<sub>4</sub> MNPs,<sup>155</sup> Fe<sub>3</sub>O<sub>4</sub>-GO composites,<sup>156</sup> CeO<sub>2</sub>-coated hollow Fe<sub>3</sub>O<sub>4</sub> nanocomposites,<sup>157</sup>) and iron-containing nanomaterials (e.g., assembling hemin in ZIF-8<sup>18</sup>) have widely been used for glucose detection. In all the cases, these materials were combined with GOx and synergistic effect of these two enzymes was the key factor in achieving high sensitivity and superior analytical performance in biomolecular sensing. Again, the sensitivity of glucose detection can also be increased by introducing pores to the iron oxide nanoparticles as it increases the effective catalytic surface area and exposes the metal ions to the surface. For instance, Masud *et al.* detected glucose concentration as low as 0.9 μM with the mesoporous iron oxide (γ-Fe<sub>2</sub>O<sub>3</sub>), which is ten-times more sensitive than that of the assay with the ZIF-8 (NiPd) nanoflowers.<sup>158</sup> In addition to porosity, oxidation state of the metal could also influence the nanozyme activity. LaNiO<sub>3</sub> perovskite with Ni<sup>3+</sup> demonstrated 58-fold and 22-fold higher peroxidase activity than that of perovskite with Ni<sup>2+</sup> (e.g., NiO nanoparticles) and Ni<sup>0</sup> (e.g., Ni nanoparticles) oxidation states, respectively. In addition to porosity, oxidation state could influence the activity of nanozymes. LaNiO<sub>3</sub> perovskite with Ni<sup>3+</sup> demonstrated 58~fold and 22~fold higher peroxidase activity than that of nanoparticle with Ni<sup>2+</sup> (e.g., NiO nanoparticles) and Ni<sup>0</sup> (e.g., Ni nanoparticles) oxidation states, respectively. The superior activity of these nanozymes facilitated the colorimetric assays of H<sub>2</sub>O<sub>2</sub>, glucose, and sarcosine.<sup>159</sup> However, as described by Wang *et al.*, the occupancy of *e<sub>g</sub>* orbitals of the central metal ions may affect the peroxidase-like activity of perovskite nanozyme.<sup>160</sup>

In recent years, nanozymes have also been used in colorimetric detection of DNA methylation<sup>161</sup>, a potential epigenetic biomarker. Shiddiky group has developed a unique method for detecting DNA methylation using the peroxidase-like activity of the mesoporous iron oxides.<sup>53</sup> In this assay, the target DNA samples were extracted and denatured prior to their adsorption onto the surface of a bare screen-printed gold electrode (SPGE) via gold-DNA affinity interaction. 5-methyl cytosine antibody (5mC) functionalized mesoporous iron oxide nanozymes were then used to recognise the methyl cytosine groups present on the SPGE. The nanozymes catalyze the TMB in the presence of H<sub>2</sub>O<sub>2</sub> to give the colorimetric (i.e., naked-eye observation) and electrochemical quantification of methylation level. The assay could successfully detect as low as 10% difference of global DNA methylation level in synthetic samples and cell lines with good reproducibility and specificity (% RSD = <5%, for n = 3).

Modulation of peroxidase-like activity of nanozymes via interacting with molecules and ions present in biological systems can be used to detect biomolecular targets. Shah *et al.* used the interaction of AuNPs nanozymes with ATP, ADP, carbonate, sulphate and phosphate ions and the resultant peroxidase-like activity was calculated.<sup>162</sup> It was shown that compared to ADP, phosphate, sulphate and carbonate ions, the incorporation of ATP in the system could significantly enhance the nanozyme activity of AuNPs nanozymes. On the contrary, surface passivation of citrate-capped AuNPs with DNA aptamer inhibits peroxidase substrate to reach the AuNPs surface, thereby attenuates their nanozyme activity. However, when the aptamer binds to its specific targets, it leaves the AuNPs surface and reactivates the nanozyme activity. Based on this phenomenon, Weerathunge *et al.* used AuNP-aptamer transducer to detect murine norovirus with a detection limit of 3 viruses (~30 viruses/mL) within 10 min.<sup>21</sup> As the method

can be used for other aptamers (i.e., it is not limited to any specific aptamers), this AuNPs nanozyme-based sensor can be adopted for the detection of other viruses.

### 5.3 Fluorescence sensor

A fluorescence sensor consists of the emission of light by a material (fluorophore) after being excited at lower wavelengths and the intensity (or lifetime) of that emission varies with the concentration of the target analyte.<sup>163</sup> In this type of sensor, nanozyme converts a non-fluorescent substrate into a fluorescently active one by catalysing hydrolysis or oxidation reaction. For instance, it was reported that iron and nitrogen-incorporated CNTs that were grown *in situ* on 3D porous carbon foam (denoted as Fe-Phen-CFs) possesses a peroxidase-like activity, which could oxidise terephthalic acid (TA) to the fluorescent product of hydroxyl terephthalate (HTA) in the presence of  $\text{H}_2\text{O}_2$  and can be used as a unique strategy for fluorescence detection of  $\text{H}_2\text{O}_2$ .<sup>164</sup> However, similar to other peroxidase-mimic nanozymes, Fe-Phen-CFs needs to be coupled with GOx. The method showed excellent sensitivity towards the detection of  $\text{H}_2\text{O}_2$  and glucose with a detection limit of 68 nM and 0.19 mM, respectively.

In recent years, the ratiometric fluorescence sensor has gained popularity because of its built-in self-calibration for signal correction, enabling more reliable detection. It also enables more accurate imaging contrast, which often leads to higher detection sensitivity. Ratiometric fluorescence sensor can effectively overcome most of the issues associated with false positive results in traditional fluorescence sensing by introducing another fluorescence emission band to achieve ratiometric signal readouts.<sup>165-166</sup> Very recently, this sensor has been used for the detection of  $\text{H}_2\text{O}_2$  and glucose. Briefly, the peroxidase-like activity of ruthenium ion/carbon nitride ( $\text{Ru}-\text{C}_3\text{N}_4$ ) nanosheets catalyses OPD to fluorescent DAB which exhibits emission at 565

nm. Meanwhile, fluorescence emission at 455 nm by Ru-C<sub>3</sub>N<sub>4</sub> decreases or quenches due to the inner filter effect of the generated DAB. Via this method, an excellent sensitivity and selectivity to serum glucose in the presence of common interferences were obtained.<sup>166</sup>

## **6. Applications of nanozyme-based electrochemical biosensors**

An electrochemical biosensor provides a suitable platform that facilitates the formation of probe-target complex (i.e., specific recognition event) in such a way that the binding event triggers a useable signal for electrochemical readout.<sup>167</sup> Over the past several decades, electrochemical biosensors have successfully been used in detecting a range of molecular and cellular biomarkers in the fields of biomedical, biotechnology, and environmental sciences. Most importantly, the electrochemical detection system is amenable to miniaturization and offers other advantages such as simplicity, cost-effective nature, high sensitivity and specificity.<sup>168</sup> As shown in **Figure 4**, biorecognition and signal transduction are two critical elements in the fabrication of electrochemical biosensors, and nanozyme have played an essential role in this regard.

### **6.1 Genosensor**

Detection of specific nucleic acid (DNA or RNA) sequences has proved their utility in molecular diagnostics, pathogen detection and nanomedicine (nanoscience and nanotechnology) applications in the life and health sciences. It is known that many malignant diseases (e.g., cancer) and pathogenic infections present their signature nucleic acid markers (e.g., circulating tumor DNA, microRNA) in the peripheral circulatory system which can be used as diagnostics, prognostics and therapeutic markers.<sup>169,170</sup> The concentration of these circulating biomarkers in the peripheral blood or other bodily fluids (saliva, urine, etc.) is extremely low at the early

stages of the diseases.<sup>170</sup> Therefore, highly sensitive and specific analysis/detection methods are required. To achieve this goal, nanozymes-based catalytic signal amplification strategy for nucleic acid detection is one of the promising options.

In electrochemical nucleic acid biosensor, sensitivity can easily be enhanced via incorporating catalytic hairpin assembly (CHA) combined with nanozyme label-based redox cycling signal amplification. As outlined by Hun *et al.*, CHA was used to form a double stranded DNA on a AuNPs modified electrode.<sup>70</sup> Initially, hairpin H1 was immobilized onto AuNPs modified gold electrodes and in the presence of the target DNA, the stem-loop structure of H1 opened due to binding to the target DNA and formed a double strand product with 21 base hybridization. This triggered in the opening of the second hairpin and formed the partially complementary dsDNA with 39 base hybridization. This step released the target DNA which could be recycled and used for opening another H1. In the second step, DNA probe functionalized Au@PtNPs nanocatalyst was hybridized with the electrode attached DNA. Au@PtNPs can catalyze the reduction of p-nitrophenol (PNP) to p-aminophenol (PAP) in the presence of NaBH<sub>4</sub>. The generated PAP was electrooxidized to p-quinone imine (PQI) by ferrocenecarboxylic acid (FCA) in the solution. The produced PQI was then reduced back to PAP by NaBH<sub>4</sub>, leading to the redox cycling between PAP and PQI. As a result, an enhanced electrochemical response was produces which allows to achieve a high sensitivity with 3-orders of magnitude higher than that of AuNP labels alone. This sensor was able to detect as low as 0.3aM DNA. In another strategy, Ling *et al.* reported an electrochemical DNA quantification method based on nanozyme activity of MOF nanostructure and allosteric switch of hairpin DNA (**Figure 5**).<sup>69</sup> Initially, glassy carbon electrode was functionalized with the streptavidin (SA) aptamer sequence of a hairpin DNA. Due to its loop structure, electrode-bound hairpin DNA is



inaccessible to SA attached conjugates. Upon the addition of target DNA, the loop bound to the target sequence and unfolded the stem of hairpin DNA, making it accessible for SA attached conjugates to form a structure with the combinative SA aptamer. The surface-bound activated DNA was selectively bind with the SA coated FeTCPP@MOF via specific interaction between SA-apatamer and SA. Nanozyme activity of FeTCPP@MOF was then used to catalyse the oxidation of o-phenylenediamine (o-PD) in the presence of H<sub>2</sub>O<sub>2</sub>. This assay demonstrates a good performance for the detection of DNA with a LOD down to 0.48 fM, the 6-order magnitude linear range, single mismatch differentiation ability, and practical application in complex samples. This study opens up a new direction of functionalized MOF as nanozymes for signal transduction in electrochemical biosensing and shows better enzymatic activities due to their natural enzyme-like metal center and porous nanostructure.

MicroRNAs (miRNAs) are small (~17–25 nucleotides long), single-stranded noncoding RNA molecules that suppress the expression of protein-coding genes by translational repression, messenger RNA degradation, or both and involved in early events in disease progression.<sup>172,173</sup> In recent years, circulating miRNAs and exosomal miRNAs (exo-miRNA) have been used as diagnostic and prognostic markers for a range of diseases, including cancer.<sup>174–177</sup> Quantitative real-time PCR (q-PCR), reverse transcription polymerase chain reaction (qRT-PCR), *in-situ* hybridization, northern blotting, RNA-seq analysis, microarray, next-generation sequencing are some of the techniques that have been widely used for the quantification of RNA markers in bodily fluids. These techniques are particularly suitable for biomarker discovery, and none of this technology serves the purpose of on-site or POC detection.<sup>178</sup> On the contrary, the nanozyme based electrochemical miRNA sensor provides rapid analysis along with adequate sensitivity. Li *et al.* developed a miRNA sensor to detect miRNA-122,<sup>67</sup> a biomarker of drug-induced liver

injury. The nanozyme activity of palladium nanoparticles based MOF nanohybrids was used. The nanohybrid enzymes were utilized both as nanocarriers to immobilize a large amount of biotin-labeled signal probes (H2) and as tracers to quickly catalyze the oxidation of TMB in the presence of H<sub>2</sub>O<sub>2</sub>. The target miR-122 was sandwiched between the tracers and electrode-bound thiolated capture probes (H1). With the help of target-catalyzed hairpin assembly (TCHA), target miR-122 triggered the hybridization of H1 and H2 to further released to initiate the next reaction process resulting in numerous tracers anchored onto the sensing interfaces. Due to dual signal amplification (e.g., target induced signal amplification and TMB oxidation by tracer indicator PdNPs@Fe-MOF), this method could detect miRNA-122 as low as 0.003 fM in human serum.<sup>67</sup>

## 6.2 Cytosensor

Circulating tumor cells (CTCs) have emerged as valuable tool that can provide mechanistic insights into the tumor heterogeneity, clonal evolution, and stochastic events within the metastatic cascade. They are regarded as one of the most promising biomarkers for early diagnosis of cancer.<sup>179</sup> As a general strategy of CTC detection, antibody- or aptamer-anchored (for aptasensors see Section 6.4) nanoprobe are designed to target abnormal and/or overexpressed cell surface receptors (proteins) or other cell surface components, including glycans, folic acid, and sialic acid.<sup>170,179</sup> However, the low abundance (1–10 CTCs per 1 billion of blood cells)<sup>179</sup> and inherent fragility of CTCs pose great challenges for CTC detection. To enhance the sensitivity of CTCs analysis, Tian *et al.* has developed an ultrasensitive electrochemical sensor using reduced graphene oxide/molybdenum disulfide (rGO/MoS<sub>2</sub>) composites modified magnetic glassy carbon electrode (MGCE) as a detector, and aptamer modified magnetic Fe<sub>3</sub>O<sub>4</sub>NPs as dispersible capture agents.<sup>82</sup> Cancer cells were attached with the

aptamer modified Fe<sub>3</sub>O<sub>4</sub>NPs via aptamer-antigen interaction. The cell-attached conjugates were then magnetically attached onto the rGO/MoS<sub>2</sub> composites-modified electrode. An enhanced electrochemical signal was achieved due to the nanozyme catalytic oxidation of TMB on rGO/MoS<sub>2</sub> composites with Fe<sub>3</sub>O<sub>4</sub>NPs binanozyme surface. The method was able to detect 6 MCF-7 cells per mL which showed significant improvement from their previous report with rGO/AuNPs modified GCE and MUC-1 aptamer modified CuO nanozyme (LOD 27 cells per mL).<sup>58</sup> Very recently, Alizadeh *et al.* proposed a “signal-off” strategy to detect cancer cells. CuO/WO<sub>3</sub> nanoparticle decorated graphene oxide nanosheets (CuO/WO<sub>3</sub>-GO) were modified with folic acid (FA), which were then absorbed on cancer cells via folic acid targeting ligand. In this strategy, peroxidase like-activity of CuO/WO<sub>3</sub>-GO was used to oxidise o-phenylenediamine in the presence of H<sub>2</sub>O<sub>2</sub>. During interaction between cells and CuO/WO<sub>3</sub>-GO, some amount of H<sub>2</sub>O<sub>2</sub>-OPD system participated in chemical reaction and removed from the electrode, resulting in a decrease in the response signal. Using this principle, the authors successfully achieved a detection limit of 18 cells per mL.<sup>29</sup>

### 6.3 Immunosensor

The basis of electrochemical immunosensor is the non-covalent interaction between an antigen and antibody to form a sandwich-type architecture on the electrode surface. In a conventional system, enzyme-labelled antibody or antigen amplifies the immune-capture event that can be quantified by voltammetric or amperometric readout methods.<sup>170,180</sup> In this regard, successful conjugation of antibody or antigen with enzyme is crucial. However, most of the standard conjugation, separation and purification methods for enzyme-conjugated antibody or antigens suffer from expensive, time consuming, multistep and laborious procedures. For

examples, during the conjugation of antibody with nanozyme, nearly all nanozyme labelled antibody settle down through centrifugation at relatively lower RPM, which adds an extra degree of complexity to the immunosensor fabrication process. Nanozyme-antibody conjugation can be achieved via either electrostatic interactions between the them or chemical reactions between the carboxylic acid (-COOH) or anime (-NH<sub>2</sub>) groups of functionalized nanozymes with the -NH<sub>2</sub> acid -COOH groups of antibody. For instance, it was reported that -NH<sub>2</sub> groups of secondary antibodies (Ab<sub>2</sub>) electrostatically interacted with Au@Pt (Au-N and Pt-N) of Co<sub>3</sub>O<sub>4</sub>@CeO<sub>2</sub>-Au@Pt nanozymes and used as labels in a sandwich-type electrochemical immunosensor to detect squamous cell carcinoma antigen. This sensor showcased an excellent sensitivity due to the surface area for Ab<sub>2</sub> immobilization and the synergic effect of Co<sub>3</sub>O<sub>4</sub>@CeO<sub>2</sub>-Au@Pt nanozyme towards H<sub>2</sub>O<sub>2</sub> reduction. This assay offered a LOD of 33 fg per mL.<sup>181</sup> Wei et al also published a similar approach for the quantitative detection of hepatitis B surface antigen using MoS<sub>2</sub>@Cu<sub>2</sub>O-Pt nanozymes.<sup>182</sup>

Although nanozyme-based sensors are well known for amplifying the readout signals (i.e., “signal-on”), they can equally be useful in generating a noticeable change in electrochemical response in “signal-off” sandwich immunosensing strategies. This method generally involves a nanozyme catalyzed chemical reaction that forms a nonconducting precipitate on the electrode surface. The precipitate blocks the working area of the electrode and thus hinders the electron transfer reaction between the solution-phase electroactive species and electrode. In some cases, the precipitate may reduce the concentration of the electroactive species (see Section 6.2). For instance, Zhang *et al.* developed a “signal-off” sandwich immunosensor to detect  $\alpha$ -fetoprotein. After the successful immune-recognition of FeS<sub>2</sub>-AuNPs-Ab<sub>2</sub> on the electrode surface, FeS<sub>2</sub>-AuNPs nanozymes catalyze 4-chloro-1-naphthol in the presence of H<sub>2</sub>O<sub>2</sub> to form insoluble

precipitation. Thus, a reduced differential pulse voltammetric response of electroactive nickel hexacyanoferrate nanoparticles (NiHCFNPs) was observed.<sup>183</sup>

Recently Shiddiky group has developed an immunosensor to detect p53 autoantibody in serum and highlighted that the method could be adopted for virtually any type of protein biomarkers.<sup>54</sup> In this method, the surface of a new class of nanozyme, gold-loaded nanoporous Fe<sub>2</sub>O<sub>3</sub> nanocube (Au-NPFe<sub>2</sub>O<sub>3</sub>NC), was modified with IgG and used them as labels in sandwich immunodetection of autoantibody. As shown in **Figure 6**, a biotinylated p53 antigen was attached to neutravidin-modified screen-printed carbon electrode via biotin-neutravidin affinity interaction. This electrode was then incubated with the serum sample to capture the target p53 autoantibody present within the sample. The IgG/Au-NPFe<sub>2</sub>O<sub>3</sub>NC is used to recognize electrode-bound autoantibodies. The nanozyme activity of IgG/Au-NPFe<sub>2</sub>O<sub>3</sub>NC was to adopt an ELISA-based sensing protocol where the oxidation of TMB in the presence of hydrogen peroxide was mimicked to generate coloured complexes for naked-eye observation and electrochemical detection of target autoantibodies. The electrochemical quantification has been carried out using a new screen-printed electrode. The most attractive feature of this sensor is that the high surface area and enhanced nanozyme activity of the Au-NPFe<sub>2</sub>O<sub>3</sub>NC offer enhanced sensitivity (i.e., LOD of 0.08U/mL) in immunodetection of autoantibody in biological fluids. Although this sensitivity is enough to detect p53 autoantibody in the clinical sample, it cannot obsolete the HRP based sensor having a LOD of 0.02U/mL, previously reported by the same group.<sup>54,73</sup>

The nanozyme activity of Au-NPFe<sub>2</sub>O<sub>3</sub>NC has been used to develop a simple method for direct isolation and subsequent detection of a specific population of exosomes.<sup>55</sup> In this method, the Au-NPFe<sub>2</sub>O<sub>3</sub>NC were initially functionalized with a generic exosomes-associated antibody

(i.e., CD63) and dispersed in the target samples where they work as “dispersible nanocarriers” to capture the bulk population of exosomes. After magnetic collection and purification, Au–NPFe<sub>2</sub>O<sub>3</sub>NC-bound exosomes were transferred to the disease-specific antibody-modified electrode. As a proof of principle, they used a specific placental marker, placenta alkaline phosphatase (PLAP), to detect exosomes secreted from placental cells. The nanozyme activity of Au–NPFe<sub>2</sub>O<sub>3</sub>NC was then used to accomplish a naked-eye observation along with UV–visible and electrochemical detection of PLAP-specific exosomes present in placental cell-conditioned media. They showed an excellent agreement in analytical performance for their methods using with and without commercial “total exosome isolation kit”-based pre-isolation step.

Shiddiky group also developed another class of mesoporous iron oxide materials and demonstrated their nanozyme activity in immune detection of DNA methylation.<sup>53</sup> In this method, the target DNA was first extracted and denatured to get ssDNA followed by direct adsorption onto the surface of a bare screen-printed gold electrode. A 5-methylcytosine antibody (5mC) functionalized mesoporous iron oxide materials were then used to recognize the methyl cytosine groups present on the electrode. The nanozyme-5mC conjugates catalyse the TMB solution to give the naked-eye observation and electrochemical detection of DNA methylation. The assay successfully detected as low as 10% difference in the global DNA methylation level in synthetic samples and cell lines with good reproducibility and specificity. This strategy avoids the use of HRP, traditional PCR based amplification and bisulfite treatment steps that are generally used in many conventional DNA methylation assays.

## **6.4 Aptasensor**

Aptamers are ssDNA or RNA molecules synthesized by SELEX (systematized exponentially enriched ligands) with a unique two- or three-dimensional structure that bind to a specific target molecule.<sup>184</sup> Due to their strong affinity (i.e., high specificity to target), small size, excellent stability, and flexibility in modification, aptamers become a strong competitor of antibody.<sup>21,50,185</sup> In recent years, nanozyme conjugated aptamers have been used for detecting whole-cell,<sup>58</sup> pathogen,<sup>50</sup> and protein<sup>75,76,79</sup>. Sun *et al.* developed a method to detect cardiac troponin I (cTnI), a gold standard marker for acute myocardial infarction (AMI) found in the bloodstream, where nanozymes were used for catalytic signal enhancement. This sensor was fabricated by immobilizing nanotetrahedron (NTH) based dual aptamers (Tro4 and Tro6) on the screen-printed gold electrode.<sup>75</sup> After binding of target (cTnI) aptamers modified Fe<sub>3</sub>O<sub>4</sub>@UiO-66/Cu@Au (nanoprobe-1), it was dispensed on the electrode surface to form super-sandwich-like structure. Nanoprobe-1 could oxidize HQ in the presence of H<sub>2</sub>O<sub>2</sub> through multiple nanozyme activities attributed to Fe<sub>3</sub>O<sub>4</sub>@UiO-66 and Cu@Au (**Figure 7**). Additionally, attachment of super-sandwich and cDNA (complementary to aptamers) modified Cu@Au through hybridization forms a cluster-based nanoprobe, which could further increase the catalytically active sites for the HQ/H<sub>2</sub>O<sub>2</sub> system, resulting in a more sensitive catalytic response.<sup>75</sup> A more sensitive electrochemical assay for the detection of cTnI was fabricated using co-catalysis of magnetic Fe<sub>3</sub>O<sub>4</sub> nanocarriers loaded with natural HRP, Au@Pt nanozyme and G-quadruplex/hemin DNAzyme (7.5 vs. 16 pg per mL).<sup>74</sup> In both of the cases, NTH helps to maintain precise orientation of aptamers on the sensing surfaces, providing native-like microenvironment for cTnI binding.

Recently, gold nanozyme based aptasensors have been developed for detection of pathogens.<sup>21</sup> In 2019, Bansal group developed an electrochemical sensor for the detection of

*Pseudomonas aeruginosa* (PA) bacterial pathogen using the nanozyme activity of AuNPs and high affinity and specificity of a PA-specific aptamer (F23).<sup>50</sup> The presence of aptamer inhibits the inherent peroxidase-like activity of GNPs by simple adsorption on to the surface of GNPs. In the presence of target pathogens, the aptamer leaves the AuNPs surface, allowing them to resume their peroxidase-like activity, resulting in oxidation of TMB at screen-printed carbon electrode. The method is sensitive to detect PA with a LOD of ~ 60 CFU per mL in water within 10 min. The authors envisaged that this assay might become a generic platform to detect other molecular and cellular analytes.

## 6.5 Small molecule detection

Small molecules include heavy metal ions and low molecular weight organic compounds such as drugs, toxins (e.g., ochratoxin A), pesticides, antibiotics (e.g., kanamycin A), amino acids (e.g., biothiols: cysteine, glutathione), intermediate of sugars (e.g., glucose), lipids (e.g., cholesterol), second messengers (e.g., cAMP, cGMP), metabolite of cellular respiration (e.g., lactate) etc.<sup>186-189</sup> Some of these molecules are essential biomarkers for many diseases. Thus, measuring the concentration of a given small molecule in bodily fluids (i.e. whole blood, serum, urine, saliva, tear, and sweat) is an effective way to diagnose a disease. For example, blood glucose level is an indicator of diabetes: hyperglycemia and hypoglycemia,<sup>190-191</sup> blood lactate level can predict multiple system organ failure (MSOF) caused by septic shock<sup>192</sup> and ischemia and inadequate oxygenation<sup>193</sup>. Over the years, a number of enzyme-mimicking nanostructured materials<sup>188, 193-204</sup> have been used for the detection of glucose,<sup>194-197, 202, 203</sup> lactate,<sup>193, 198-199, 204</sup> uric acids,<sup>200</sup> kanamycin,<sup>188</sup> and arsenite<sup>201</sup>. In this section, nanozyme based electrochemical sensor for glucose detection is briefly discussed.



Majority of electrochemical glucose sensors worked based on the direct enzymatic oxidation of  $\text{H}_2\text{O}_2$  at GOx-modified electrode. This design commonly suffers from the interference of ascorbic acid (AA), uric acid(UA), 4-acetaminophen (AP) and other electroactive species present in the blood. This problem can be avoided by using the enzymatic reduction of  $\text{H}_2\text{O}_2$  at relatively low potential. Gao *et al.* developed a glucose sensor based on the co-immobilizing of Prussian blue (PB) and GOx on  $\text{TiO}_2$  nanotube arrays (TiNTs).<sup>203</sup> In this assay, PB reduced  $\text{H}_2\text{O}_2$  at relatively low potential. The sensor demonstrated not only high selectivity to glucose but also fast response (1 sec) and broad dynamic range (0.01 to 0.70 mM) with a detection limit of 3.2 mM. Recently, Shiddiky group reported a dual-mode (colorimetric and electrochemical) glucose sensor, where the peroxidase-mimicking activity of mesoporous  $\text{Fe}_2\text{O}_3$  nanozyme was used to catalyse the oxidation of TMB in the presence of in-situ enzymatically produced  $\text{H}_2\text{O}_2$ . Both the colorimetric (naked-eye and UV-vis) and electrochemical assays estimated the glucose concentration to be in the linear range from 1.0  $\mu\text{M}$  to 100  $\mu\text{M}$  with a detection limit of 1.0  $\mu\text{M}$ .<sup>194</sup>

## **7. Applications of nanozymes in microfluidic-based assays**

Microfluidics is a science and technology of handling and precise controlling of the sub-milliliter volume of fluids in micrometre-scale platforms.<sup>205,206</sup> There are several formats of microfluidics, including continuous-flow microfluidics, paper-based microfluidics (also known as microfluidic paper-based analytical devices ( $\mu\text{PADs}$ )), digital and droplet-based microfluidics.<sup>207,208</sup> The synergistic combination of these formats of microfluidics with biosensors can increase the sensitivity, selectivity and portability, while decreasing the LOD and

overall footprint, of such analytical devices.<sup>209,210</sup> Moreover, integrated, microfluidic-based biosensors can realise the real-time and multianalyte detection of various biomarkers.

Nanozymes have also been used in such microfluidic-based biosensors that function mainly based on colorimetric, fluorescent and electrochemical detection methods. One of the early works in this field was based on a versatile microfluidic device, termed as a multiplexed volumetric bar-chart chip (V-Chip).<sup>211</sup> V-Chip efficiently measured the oxygen gas produced as a result of decomposition of hydrogen peroxide in the presence of PtNPs.<sup>212</sup> Combined with the ELISA technique, it was shown that V-Chip could efficiently detect cancer biomarkers in both serum and on the cell surface. Later, this microfluidic chip was integrated with a target-responsive hydrogel containing Au@PtNPs for quantitative POC testings.<sup>213</sup>

Nanozyme-based colorimetric  $\mu$ PADs are also accessible, cost-effective and relatively simple analytical platforms that have the excellent commercialization capability in this field. Such analytical devices can be integrated with off-the-shelf equipment such as smartphones for further processing the analytical signals. For instance, Han *et al.* incorporated AuNPs in a  $\mu$ PAD to colorimetrically detect mercury ions ( $\text{Hg}^{2+}$ ) in water samples. The intensity of the colorimetric detection correlated well with the efficient reaction of Au-Hg facilitated by gold NPs in the fabricated  $\mu$ PAD. Using MOF as a peroxidase mimic to oxidase TMB in the presence of  $\text{H}_2\text{O}_2$ , a colorimetric  $\mu$ PAD-based biosensor was also developed for glucose monitoring.<sup>214</sup> The  $\mu$ PAD could also be integrated with a smartphone for quantitative analysis of the generated color. Zhang *et al.* used modified carbon nitride nanozymes for colorimetric detection of glucose.<sup>215</sup> Using a microfluidic device for real-time monitoring, their developed microfluidic platform with metal-free nanozymes could detect glucose with a LOD as low as  $0.8 \mu\text{M}$  within 30 seconds.

Through incorporating zeolitic imidazolate framework (ZIF-8) based nanozymes in an I-shaped microfluidic channel and using a fluorescent detection technique, Cheng *et al.* realized an *in vivo*, real-time, continuous biosensor platform.<sup>216</sup> To sensitively detect the secreted hydrogen peroxide from single cells, a droplet-based microfluidic platform has also been developed in the literature.<sup>217</sup> A high fluorescent signal generated with the hybridization of HRP with gold nanoclusters trapped in a 4.2 nL droplet led to the sensitive detection of H<sub>2</sub>O<sub>2</sub>.

A rapid and efficient microfluidic-based nanozyme-mediated electrochemical detection device for targeted genetic analysis was developed by Koo *et al.*<sup>218</sup> The authors fabricated an electrode-patterned microfluidic chip with one central lysis chamber and four amplification chambers. The surface of the amplification chambers was immobilized with superparamagnetic iron oxide NPs to detect circulating tumor nucleic acids (ctNA) in the urine and blood of patients with prostate cancer. An electrochemical-based microfluidic POC device for real-time detection of H<sub>2</sub>O<sub>2</sub> was also fabricated.<sup>219</sup> It was shown that stable biosensor with tremendous peroxidase-like catalytic activity and LOD as low as 1.62 μM can be realized by immobilization of gold and platinum NPs with GO inside a hydrogel microbead.

## **8. Challenges in nanozymes-based electrochemical biosensors and potential solutions**

Although nanozymes-based electrochemical biosensors are promising platforms for detecting various analytes of interest quickly and reliably, they suffer from the combined technical and clinical challenges associated with both nanozymes and electrochemical biosensors.

### **8.1 Technical challenges associated with nanozymes**

*8.1.1 Limited enzyme-mimicking activities of nanozymes:* One of the major issues of nanozymes that need continuous improvement is their enzyme-mimicking activities. To this aim, synthesizing more robust nanozymes that better exhibit the properties of natural enzymes are demanding. In particular, current advances in nanotechnology, artificial intelligence and computational chemistry can significantly improve the oxidoreductase activity of nanozymes for electrochemical detection.

*8.1.2 Low specificity of nanozymes:* The inherently low specificity of nanozymes is another limitation of nanozymes. Unlike natural enzymes, nanozymes lack precise binding sites to interact with a substrate appropriately. This issue of lacking the substrate-binding sites significantly affects the specificity of nanozymes; thus, modifications/engineering of the nanozymes are required to improve their specificity. Moreover, high specificity is critically important in biomolecular sensing for various biomedical applications, especially for disease diagnosis and monitoring. As such, nanozymes with highly improved specificity need to be used in electrochemical biosensors for disease detection.

*8.1.3 Low catalytic activities of nanozymes:* Another inherent problem of nanozymes is their relatively low catalytic activities compared to those of natural enzymes. The relatively low catalytic activities of nanozymes significantly compromise their bioconjugation. This limitation can be addressed by using molecularly imprinted polymers (MIPs) on nanozymes<sup>220</sup> as well as synthesizing the so-called integrated nanozymes.<sup>38</sup> MIPs improve the specificity and catalytic activity through generating binding sites on the substrate by polymerization. In INAZymes, the natural enzymes are combined with nanozymes in a 3D network structure to improve the

selectivity and catalytic activity. Among various 3D network structures required to fabricate such hybrid enzyme-mimicking nanomaterial, MOFs hold great promise.<sup>221</sup> Using MIP- or MOF-based hybrid nanozymes in electrochemical biosensors can significantly improve the selectivity of the system.

*8.1.4 Poor reproducibility of nanozymes:* Poor reproducibility of nanozymes is a significant problem that potentially hinders the widespread application of nanozymes-based electrochemical biosensors. This issue mainly arises for two reasons. Firstly, small-scale synthesis in the individual lab does not guarantee size, shape, and porosity of nanoparticle from different batches, leading to activity changes. Secondly, bioconjugation between recognition element and nanozyme is highly subjective and depends on an individual's expertise and considerations. Therefore, essential efforts need to be taken to make the industrial production and standardization of effective bioconjugation protocols.

## **8.2 Clinical challenges associated with nanozymes-based electrochemical biosensors**

*8.2.1 False-positive results in clinical samples:* The conductivity and catalytic activity of nanozymes can significantly improve the sensitivity of electrochemical biosensors. Nevertheless, the clinical samples, such as patients' blood and urine, contain complex biological matrices, including thousands of unwanted proteins, cells, lipids and nucleic acids. These complex biological matrices can be adsorbed nonspecifically on the surface of the electrochemical sensors and eventually lead to a false-positive result. As such, the surface of the electrochemical sensor needs to be coated with nonspecific binding agents such as bovine serum albumin (BSA) and polyethylene glycol (PEG). Moreover, the aggregation of nanozymes can also interfere with the

signal transduction, thus reducing the specificity of the biosensor. To address this issue, it is recommended that the solution containing the nanozymes be kept away from UV sources and reactive oxygen species (ROS)-rich environments. Finally, a specific recognition probe such as an aptamer-nanozyme probe can be implemented into the detection device to improve the specificity of the device.

*8.2.2 Biofouling:* Biofouling of electrode surface is a significant clinical challenge that can hinder nanozymes-based electrochemical biosensors for clinical applications. The problem of biofouling of the electrodes is more highlighted when the electrochemical biosensors are being used for detecting disease-specific biomarkers in bodily fluids. Since the electrodes are in direct contact with the bodily fluids such as blood, urine, plasma, or serum, unwanted cells, proteins, and other biomolecules may attach to the electrode surfaces via non-specific interaction. This can adversely affect the specificity and decrease the signal-to-noise ratio. To address this problem, the surface of the electrode needs to be coated with anti-fouling materials such as zwitterionic polymers, peptides, and polyethylene glycol.<sup>222</sup>

*8.2.3 Lack of standard protocols for synthesising and bioconjugation:* Although nanozymes are highly versatile, stable, and inexpensive, their synthesizing methods may differ from one lab to another. Also, the fabrications techniques of nanozymes are highly subjective, and the bioconjugation process may depend on individuals' skills. As such, nanozymes-based electrochemical biosensors may suffer from poor reproducibility, which is a crucial factor affecting their acceptance for real clinical settings. Therefore, this field can significantly benefit from standardization and automation. In this regard, the integration of these systems with

microfluidic technology can be highly beneficial and has the potential to address these limitations. For instance, the synthesizing methods of nanozymes and the bioconjugation process involve many steps of mixing, washing, and separation. These steps are usually performed using rotating lab shakers and centrifuge machines whose durations mainly differ from one lab to another. On the other hand, mixing and separation in microfluidic devices are highly efficient and can be efficiently streamlined.<sup>223</sup>

*8.2.4 Lack of an automated nanozymes-based electrochemical biosensing platform for point-of-care testing:* To address the issue of automation of nanozymes-based electrochemical biosensors for POC testing and disease detection, it would be highly demanding to integrate the whole process of isolation, separation, and detection of the pathogenic targets on the same device. This concept is closely related to lab-on-a-chip or micro total analysis systems that are currently being practised for many chronic diseases such as cancer<sup>224</sup> and autoimmune disorders.<sup>225</sup>

## **9. Concluding remarks and future perspectives**

The last decade witnessed an overwhelming surge in research about nanozymes and expanded their applications to biomedical sensing, therapeutics, and environmental engineering. Herein, we summarize the representative enzyme mimics, plausible catalytic mechanism, and a particular focus has been given to the recent updates in nanozyme based electrochemical detection of clinically relevant biomarkers (e.g., DNA, miRNA, protein, and CTCs). Dynamic progress in this field endows nanozyme with enormous functionalities such as nanocarriers, robust catalytic behaviour, probe immobilizers, conductive surface modifiers and signal generator or tracer tag. Until now, few nanozymes show catalytic activity as natural counterparts, but the majority

manifests moderate to low activity. Although heteroatom doping, composite or bimetal formation may increase the activity significantly, improvement in substrate selectivity remains low. On the other hand, molecular imprinting or surface modifications improve molecular recognition and substrate selectivity sacrificing activity. In this direction, a better understanding of structure-activity relationships, rational design of nanomaterials, experimental and computational studies are pivotal to elucidate the catalytic mechanism and impart maximum activity and selectivity at the same time or balancing them for a particular application.

One of the critical issues is the multi-enzymatic property, which has been proved to be useful in therapeutic purposes. Still, it is not properly addressed how this could be beneficial to design and fabricate solid-state immunoassays (ELISA, LFIA) and electrochemical sensors. Moreover, over the years, most of the sensors have utilized HRP-mimicking nanomaterials. Thus, the majority of nanozymes remained unexplored. The development of multifunctional nanozymes could be a challenging and interesting topic for the coming days. Besides catalysis, specific physicochemical properties such as magnetic, optical, or thermal properties would capacitate enzyme mimics to be realized for ultra-sensitive and user-friendly detection of a biomolecule from complex body fluids.

Finally, the combination of this field with microfluidics can streamline many tedious and highly-subjective processes of synthesizing and bioconjugation. For instance, replacing the laboratory shakers and centrifuge machines with efficient micromixers and microfluidic-based particle separation devices can facilitate the automation and standardization of this field. Moreover, integrating the whole process of isolation separation and detection of the pathogenic targets on a single chip can revolutionize the applications of nanozymes-based electrochemical biosensors for disease diagnosis and monitoring of the therapy effectiveness.



## **Nomenclature**

ABTS: 2,2'-Azino-bis-3(ethylbenzthiazoline-6-sulfonic acid)

Au@PtNPs: gold core/platinum shell nanoparticles

BPDE: benzo[a]pyrene-7,8-diol 9,10-epoxide

CHA: catalytic hairpin assembly

ctDNA: circulating tumor deoxyribonucleic acid

CNTs: carbon nanotubes

DAB: 3,3'-Diaminobenzidine

DNC: dextran-coated nanoceria

dsDNA: double-stranded deoxyribonucleic acid

EBOV: ebolavirus

ELISA: enzyme-linked immunosorbent assay

FCA: ferrocene carboxylic acid

GO: graphene oxide

GOx: glucose oxidase

GPx: glutathione peroxidase

HRP: horseradish peroxidase

IONPs: Iron oxide nanoparticles

IONzyme: iron oxide nanozyme

LFBs: lateral flow biosensors

LFIA: lateral flow immunochromatographic assays

MNP: magnetic nanoparticle

MOFs: metal-organic frameworks

NPs: nanoparticles

OPD: o-phenylenediamine dihydrochloride

PAP:p-aminophenol

PB: prussian blue

PQI: p-quinone imine

PNP: p-nitrophenol

PtNCs: platinum nanocatalysts

POC: point-of-care

rGO: reduced graphene oxide

SOD: superoxide dismutase

ssDNA: single-stranded deoxyribonucleic acid

TEP:triethylphosphite

TMB :3,3',5,5'-Tetramethylbenzidin

TTMPP: tris(2,4,6-trimethoxyphenyl)phosphine

### **Acknowledgement**

This work was partly supported by the Australian Research Council (ARC) Discovery Projects (DP180100055, DP190102944) and the National Research Foundation of Korea (NRF) grant (2019R1A2C1002531) funded by the Korean government.

## References

1. F. Manea, F. B. Houillon, L. Pasquato and P. Scrimin, *Angew. Chem., Int. Ed.*, 2004, **43**, 6165–6169.
2. J. Wu, X. Wang, Q. Wang, Z. Lou, S. Li, Y. Zhu, L. Qin and H. Wei, *Chem. Soc. Rev.*, 2019, **48**, 1004–1076.
3. L. Gao, J. Zhuang, L. Nie, J. Zhang, Y. Zhang, N. Gu, T. Wang, J. Feng, D. Yang, S. Perrett and X. Yan, *Nat. Nanotechnol.*, 2007, **2**, 577–583.
4. Y. Huang, J. Ren and X. Qu, *Chem. Rev.*, 2019, **119**, 4357–4412.
5. D. Jiang, D. Ni, Z. T. Rosenkrans, P. Huang, X. Yan and W. Cai, *Chem. Soc. Rev.*, 2019, **48**, 3683–3704.
6. J. Wu, S. Li and H. Wei, *Nanoscale Horiz.*, 2018, **3**, 367–382.
7. X. Zheng, Q. Liu, C. Jing, Y. Li, D. Li, W. Luo, Y. Wen, Y. He, Q. Huang, Y. T. Long and C. Fan, *Angew. Chem., Int. Ed.*, 2011, **50**, 11994–11998.
8. W. Luo, C. Zhu, S. Su, D. Li, Y. He, Q. Huang and C. Fan, *ACS Nano*, 2010, **4**, 7451–7458.
9. X. Shen, W. Liu, X. Gao, Z. Lu, X. Wu and X. Gao, *J. Am. Chem. Soc.*, 2015, **137**, 15882–15891.
10. L. Jin, Z. Meng, Y. Zhang, S. Cai, Z. Zhang, C. Li, L. Shang and Y. Shen, *ACS Appl. Mater. Interfaces*, 2017, **9**, 10027–10033.
11. Z. Gao, M. Xu, L. Hou, G. Chen and D. Tang, *Anal. Chim. Acta*, 2013, **776**, 79–86.
12. R. Polsky, R. Gill, L. Kaganovsky and I. Willner, *Anal. Chem.*, 2006, **78**, 2268–2271.
13. T. Li, Y. Du and E. Wang, *Chem.-Asian J.*, 2008, **3**, 1942–1948.
14. J. Lan, W. Xu, Q. Wan, X. Zhang, J. Lin, J. Chen and J. Chen, *Anal. Chim. Acta*, 2014, **825**, 63–68.
15. Q. Wang, X. Zhang, L. Huang, Z. Zhang and S. Dong, *Angew. Chem., Int. Ed.*, 2017, **56**, 16082–16085.
16. Y. Hu, H. Cheng, X. Zhao, J. Wu, F. Muhammad, S. Lin, J. He, L. Zhou, C. Zhang, Y. Deng, P. Wang, Z. Zhou, S. Nie and H. Wei, *ACS Nano*, 2017, **11**, 5558–5566.
17. L. Gao, K. Fan and X. Yan, *Theranostics*, 2017, **7**, 3207–3227.
18. H. Cheng, L. Zhang, J. He, W. Guo, Z. Zhou, X. Zhang, S. Nie and H. Wei, *Anal. Chem.*, 2016, **88**, 5489–5497.
19. P. Weerathunge, R. Ramanathan, R. Shukla, T. K. Sharma and V. Bansal, *Anal. Chem.*, 2014, **86**, 11937–11941.
20. R. S. Li, H. Liu, B. Bin Chen, H. Z. Zhang, C. Z. Huang and J. Wang, *Anal. Methods*, 2016, **8**, 2494–2501.
21. P. Weerathunge, R. Ramanathan, V. A. Torok, K. Hodgson, Y. Xu, R. Goodacre, B. K. Behera and V. Bansal, *Anal. Chem.*, 2019, **91**, 3270–3276.
22. T. K. Sharma, R. Ramanathan, P. Weerathunge, M. Mohammadtaheri, H. K. Daima, R. Shukla and V. Bansal, *Chem. Commun.*, 2014, **50**, 15856–15859.
23. H. Cheng, S. Lin, F. Muhammad, Y.-W. Lin and H. Wei, *ACS Sens.*, 2016, **1**, 1336–1343.
24. X. Wang, L. Qin, M. Zhou, Z. Lou and H. Wei, *Anal. Chem.*, 2018, **90**, 11696–11702.
25. Z. Zhu, Z. Guan, S. Jia, Z. Lei, S. Lin, H. Zhang, Y. Ma, Z.-Q. Tian and C. J. Yang, *Angew. Chem., Int. Ed.*, 2014, **53**, 12503–12507.
26. D. Duan, K. Fan, D. Zhang, S. Tan, M. Liang, Y. Liu, J. Zhang, P. Zhang, W. Liu, X. Qiu, G. P. Kobinger, G. F. Gao and X. Yan, *Biosens. Bioelectron.*, 2015, **74**, 134–141.

27. J. Han, L. Zhang, L. Hu, K. Xing, X. Lu, Y. Huang, J. Zhang, W. Lai and T. Chen, *J. Dairy Sci.*, 2018, **101**, 5770–5779.
28. M. I. Kim, Y. Ye, B. Y. Won, S. Shin, J. Lee and H. G. Park, *Adv. Funct. Mater.*, 2011, **21**, 2868–2875.
29. N. Alizadeh, A. Salimi, R. Hallaj, F. Fathi and F. Soleimani, *Mater. Sci. Eng. C*, 2019, **99**, 1374–1383.
30. H. Fang, Y. Pan, W. Shan, M. Guo, Z. Nie, Y. Huang and S. Yao, *Anal. Methods*, 2014, **6**, 6073–6081.
31. Q. Wang, J. Lei, S. Deng, L. Zhang and H. Ju, *Chem. Commun.*, 2013, **49**, 916–918.
32. H. Wei and E. Wang, *Chem. Soc. Rev.*, 2013, **42**, 6060–6093.
33. H. Sun, Y. Zhou, J. Ren and X. Qu, *Angew. Chem., Int. Ed.*, 2018, **57**, 9224–9237.
34. S. Singh, *Biointerphases*, 2016, **11**, 04B202.
35. E. Kuah, S. Toh, J. Yee, Q. Ma and Z. Gao, *Chem.-Eur. J.*, 2016, **22**, 8404–8430.
36. J. Golchin, K. Golchin, N. Alidadian, S. Ghaderi, S. Eslamkhah, M. Eslamkhah and A. Akbarzadeh, *Artif. Cells, Nanomed, Biotechnol.*, 2017, **45**, 1069–1076.
37. Q. Wang, H. Wei, Z. Zhang, E. Wang and S. Dong, *TrAC, Trends Anal. Chem.*, 2018, **105**, 218–224.
38. J. Wu, S. Li and H. Wei, *Chem. Commun.*, 2018, **54**, 6520–6530.
39. X. Wang, Y. Hu and H. Wei, *Inorg. Chem. Front.*, 2016, **3**, 41–60.
40. S. Lin, J. Wu, J. Yao, W. Cao, F. Muhammad and H. Wei, *Nanozymes for Biomedical Sensing Applications: From In Vitro to Living Systems*, Elsevier Inc., 2018.
41. W. Zheng and X. Jiang, *Analyst*, 2016, **141**, 1196–1208.
42. M. Liang and X. Yan, *Acc. Chem. Res.*, 2019, **52**, 2190–2200.
43. X. Yan, *Nanozymology: Connecting Biology and Nanotechnology*, Springer, Singapore, 2020.
44. S. H. H. Shokouh, A. Pezeshki, S. R. A. Raza, K. Choi, S.-W. Min, P. J. Jeon, H. S. Lee and S. Im, *ACS Nano*, 2014, **8**, 5174–5181.
45. R. Bonomi, A. Cazzolaro, A. Sansone, P. Scrimin and L. J. Prins, *Angew. Chem., Int. Ed.*, 2011, **50**, 2307–2312.
46. L. Pasquato, F. Rancan, P. Scrimin, F. Mancin and C. Frigeri, *Chem. Commun.*, 2000, **2**, 2253–2254.
47. P. Pengo, S. Polizzi, L. Pasquato and P. Scrimin, *J. Am. Chem. Soc.*, 2005, **127**, 1616–1617.
48. S. Singh, *Front. Chem.*, 2019, **7**, 46.
49. A. Rahal, A. Kumar, V. Singh, B. Yadav, R. Tiwari, S. Chakraborty and K. Dhama, *Biomed Res. Int.*, 2014, **2014**, 761264.
50. R. Das, A. Dhiman, A. Kapil, V. Bansal and T. K. Sharma, *Anal. Bioanal. Chem.*, 2019, **411**, 1229–1238.
51. J. Wang, X. jiao Chen, K. ming Liao, G. hou Wang and M. Han, *Nanoscale Res. Lett.*, 2015, **10**, 1–6.
52. S. Tanaka, Y. V. Kaneti, R. Bhattacharjee, M. N. Islam, R. Nakahata, N. Abdullah, S. I. Yusa, N.-T. Nguyen, M. J. A. Shiddiky, Y. Yamauchi and M. S. A. Hossain, *ACS Appl. Mater. Interfaces*, 2018, **10**, 1039–1049.
53. R. Bhattacharjee, S. Tanaka, S. Moriam, M. K. Masud, J. Lin, S. M. Alshehri, T. Ahamad, R. R. Salunkhe, N.-T. Nguyen, Y. Yamauchi, M. S. A. Hossain and M. J. A. Shiddiky, *J. Mater. Chem. B*, 2018, **6**, 4783–4791.

54. M. K. Masud, S. Yadav, M. N. Islam, N.-T. Nguyen, C. Salomon, R. Kline, H. R. Alamri, Z. A. Allothman, Y. Yamauchi, M. S. A. Hossain and M. J. A. Shiddiky, *Anal. Chem.*, 2017, **89**, 11005–11013.
55. K. Boriachek, M. K. Masud, C. Palma, H.-P. Phan, Y. Yamauchi, M. S. A. Hossain, N.-T. Nguyen, C. Salomon and M. J. A. Shiddiky, *Anal. Chem.*, 2019, **91**, 3827–3834.
56. Z. Zhang, H. Zhu, X. Wang and X. Yang, *Microchim. Acta*, 2011, **174**, 183–189.
57. J. Mu, X. Zhao, J. Li, E. C. Yang and X. J. Zhao, *Mater. Sci. Eng. C*, 2017, **74**, 434–442.
58. L. Tian, J. Qi, K. Qian, O. Oderinde, Q. Liu, C. Yao, W. Song and Y. Wang, *J. Electroanal. Chem.*, 2018, **812**, 1–9.
59. K. Shim, W. C. Lee, M. S. Park, M. Shahabuddin, Y. Yamauchi, M. S. A. Hossain, Y.-B. Shim and J. H. Kim, *Sens. Actuators, B*, 2019, **278**, 88–96.
60. M. H. Naveen, N. G. Gurudatt, H. B. Noh and Y.-B. Shim, *Adv. Funct. Mater.*, 2016, **26**, 1590–1601.
61. H. B. Noh, K. S. Lee, P. Chandra, M. S. Won and Y.-B. Shim, *Electrochim. Acta*, 2012, **61**, 36–43.
62. G. H. Jin, E. Ko, M. K. Kim, V. K. Tran, S. E. Son, Y. Geng, W. Hur and G. H. Seong, *Sens. Actuators, B*, 2018, **274**, 201–209.
63. L. Liu, J. Du, W.-e. Liu, Y. Guo, G. Wu, W. Qi and X. Lu, *Anal. Bioanal. Chem.*, 2019, **411**, 2189–2200.
64. A. Umar, S. Kim, R. Kumar, H. Algarni and M. S. Al-Assiri, *Ceram. Int.*, 2016, **42**, 9257–9263.
65. L. Cui, J. Wu, J. Li and H. Ju, *Anal. Chem.*, 2015, **87**, 10635–10641.
66. N. Yu, Z. Wang, C. Wang, J. Han and H. Bu, *Anal. Chim. Acta*, 2017, **962**, 24–31.
67. Y. Li, C. Yu, B. Yang, Z. Liu, P. Xia and Q. Wang, *Biosens. Bioelectron.*, 2018, **102**, 307–315.
68. L. Tian, J. Qi, O. Oderinde, C. Yao, W. Song and Y. Wang, *Biosens. Bioelectron.*, 2018, **110**, 110–117.
69. P. Ling, J. Lei, L. Zhang and H. Ju, *Anal. Chem.*, 2015, **87**, 3957–3963.
70. X. Hun, G. Xie and X. Luo, *Chem. Commun.*, 2015, **51**, 7100–7103.
71. G.-Y. Zhang, S.-Y. Deng, W.-R. Cai, S. Cosnier, X.-J. Zhang and D. Shan, *Anal. Chem.*, 2015, **87**, 9093–9100.
72. L. Shi, Y. Yu, Z. Chen, L. Zhang, S. He, Q. Shi and H. Yang, *RSC Adv.*, 2015, **5**, 11541–11548.
73. S. Yadav, M. K. Masud, M. N. Islam, V. Gopalan, A. K.-Y. Lam, S. Tanaka, N.-T. Nguyen, M. S. A. Hossain, C. Li, Y. Yamauchi and M. J. A. Shiddiky, *Nanoscale*, 2017, **9**, 8805–8814.
74. D. Sun, X. Lin, J. Lu, P. Wei, Z. Luo, X. Lu, Z. Chen and L. Zhang, *Biosens. Bioelectron.*, 2019, **142**, 111578.
75. D. Sun, Z. Luo, J. Lu, S. Zhang, T. Che, Z. Chen and L. Zhang, *Biosens. Bioelectron.*, 2019, **134**, 49–56.
76. D. Ou, D. Sun, X. Lin, Z. Liang, Y. Zhong and Z. Chen, *J. Mater. Chem. B*, 2019, **7**, 3661–3669.
77. L. Jiao, Z. Mu, L. Miao, W. Du, Q. Wei and H. Li, *Microchim. Acta*, 2017, **184**, 423–429.
78. T. Zhang, Y. Song, Y. Xing, Y. Gu, X. Yan, H. Liu, N. Lu, H. Xu, Z. Xu, Z. Zhang and M. Yang, *Nanoscale*, 2019, **11**, 20221–20227.

79. Y. Wang, Y. Wang, X. Pang, B. Du, H. Li, D. Wu and Q. Wei, *Sens. Actuators, B*, 2015, **214**, 124–131.
80. P. Ling, C. Qian, J. Yu and F. Gao, *Biosens. Bioelectron.*, 2020, **149**, 111838.
81. J. Xi, C. Xie, Y. Zhang, L. Wang, J. Xiao, X. Duan, J. Ren, F. Xiao and S. Wang, *ACS Appl. Mater. Interfaces*, 2016, **8**, 22563–22573.
82. L. Tian, J. Qi, K. Qian, O. Oderinde, Y. Cai, C. Yao, W. Song and Y. Wang, *Sens. Actuators, B*, 2018, **260**, 676–684.
83. S. Savas and Z. Altintas, *Materials (Basel)*, 2019, **12**, 2189
84. M.-Q. Wang, C. Ye, S.-J. Bao, M.-W. Xu, Y. Zhang, L. Wang, X.-Q. Ma, J. Guo and C.-M. Li, *Biosens. Bioelectron.*, 2017, **87**, 998–1004.
85. X. Cai, Z. Wang, H. Zhang, Y. Li, K. Chen, H. Zhao and M. Lan, *J. Mater. Chem. B*, 2019, **7**, 401–407.
86. X. Chen, D. Liu, G. Cao, Y. Tang and C. Wu, *ACS Appl. Mater. Interfaces*, 2019, **11**, 9374–9384.
87. S. E. Son, E. Ko, V.-K. Tran, W. Hur, H. Choi, H. B. Lee, Y. Park and G. H. Seong, *ChemElectroChem*, 2019, **6**, 4666–4673.
88. J. Zhu, X. Peng, W. Nie, Y. Wang, J. Gao, W. Wen, J. N. Selvaraj, X. Zhang and S. Wang, *Biosens. Bioelectron.*, 2019, **141**, 111450.
89. K. Wang, C. Wu, F. Wang, M. Liao and G. Jiang, *Biosens. Bioelectron.*, 2020, **150**, 111869.
90. J. W. Lee, H. J. Jeon, H.-J. Shin and J. K. Kang, *Chem. Commun*, 2012, **48**, 422–424.
91. N. Puvvada, P. K. Panigrahi, D. Mandal and A. Pathak, *RSC Adv.*, 2012, **2**, 3270–3273.
92. C. Ge, G. Fang, X. Shen, Y. Chong, W. G. Wamer, X. Gao, Z. Chai, C. Chen and J.-J. Yin, *ACS Nano*, 2016, **10**, 10436–10445.
93. S. Wang, W. Chen, A. L. Liu, L. Hong, H. H. Deng and X. H. Lin, *ChemPhysChem*, 2012, **13**, 1199–1204.
94. N. Abu Tarboush, L. M. R. Jensen, M. Feng, H. Tachikawa, C. M. Wilmot and V. L. Davidson, *Biochemistry*, 2010, **49**, 9783–9791.
95. J. Xu, H. Yang, W. Fu, K. Du, Y. Sui, J. Chen, Y. Zeng, M. Li and G. Zou, *J. Magn. Mater.*, 2007, **309**, 307–311.
96. N. M. A. Rashid, C. Haw, W. Chiu, N. H. Khanis, A. Rohaizad, P. Khiew and S. A. Rahman, *CrystEngComm*, 2016, **18**, 4720–4732.
97. J. Park, K. An, Y. Hwang, J.-G. Park, H.-J. Noh, J.-Y. Kim, J.-H. Park, N.-M. Hwang and T. Hyeon, *Nat. Mater.*, 2004, **3**, 891–895.
98. S. Sun, H. Zeng, D. B. Robinson, S. Raoux, P. M. Rice, S. X. Wang and G. Li, *J. Am. Chem. Soc.*, 2004, **126**, 273–279.
99. M. E. Franke, T. J. Koplín and U. Simon, *Small*, 2006, **2**, 36–50.
100. S. Brovelli, N. Chiodini, R. Lorenzi, A. Lauria, M. Romagnoli and A. Paleari, *Nat. Commun.*, 2012, **3**, 690.
101. Z. Zhang, C. Dong, C. Yang, D. Hu, J. Long, L. Wang, H. Li, Y. Chen and D. Kong, *Adv. Synth. Catal.*, 2010, **352**, 1600–1604.
102. V. Urbanova, M. Magro, A. Gedanken, D. Baratella, F. Vianello and R. Zboril, *Chem. Mater.*, 2014, **26**, 6653–6673.
103. H. D. Yu, M. D. Regulacio, E. Ye and M. Y. Han, *Chem. Soc. Rev.*, 2013, **42**, 6006–6018.

104. M. Ambrosi, E. Fratini, P. Canton, S. Dankesreiter and P. Baglioni, *J. Mater. Chem.*, 2012, **22**, 23497–23505.
105. A. M. Ealias and M. P. Saravanakumar, *IOP Conf. Ser. Mater. Sci. Eng.*, 2017, **263**, 032019.
106. S. Sun, H. Zeng, D. B. Robinson, S. Raoux, P. M. Rice, S. X. Wang and G. Li, *J. Am. Chem. Soc.*, 2004, **126**, 273–279.
107. F. Zhao, B. Zhang and L. Feng, *Mater. Lett.*, 2012, **68**, 112–114.
108. H. Cui and W. Ren, *J. Sol-Gel Sci. Technol.*, 2008, **47**, 81–84.
109. H. Qi, B. Yan, W. Lu, C. Li and Y. Yang, *Curr. Nanosci.*, 2011, **7**, 381–388.
110. M. Sangermano, P. Allia, P. Tiberto, G. Barrera, F. Bondioli, N. Florini and M. Messori, *Macromol. Chem. Phys.*, 2013, **214**, 508–516.
111. H. Cui, Y. Liu and W. Ren, *Adv. Powder Technol.*, 2013, **24**, 93–97.
112. X.-L. Li, Q. Peng, J.-X. Yi, X. Wang and Y. Li, *Chem.-Eur. J.*, 2006, **12**, 2383–2391.
113. X. Hu, J. Gong, L. Zhang and J. C. Yu, *Adv. Mater.*, 2008, **20**, 4845–4850.
114. W.-W. Wang, Y.-J. Zhu and M.-L. Ruan, *J. Nanopart. Res.*, 2007, **9**, 419–426.
115. W.-W. Wang, Y.-J. Zhu, G.-F. Cheng and Y.-H. Huang, *Mater. Lett.*, 2006, **60**, 609–612.
116. A. V. Nikam, A. Arulkashmir, K. Krishnamoorthy, A. A. Kulkarni and B. L. V. Prasad, *Cryst. Growth Des.*, 2014, **14**, 4329–4334.
117. I. Bilecka, I. Djerdj and M. Niederberger, *Chem. Commun.*, 2008, 886–888.
118. M. I. Dar, A. K. Chandiran, M. Grätzel, M. K. Nazeeruddin and S. A. Shivashankar, *J. Mater. Chem. A*, 2014, **2**, 1662–1667.
119. T. Hyeon, S. S. Lee, J. Park, Y. Chung and H. B. Na, *J. Am. Chem. Soc.*, 2001, **123**, 12798–12801.
120. S. Guru, D. Mishra, S. S. Amritphale and S. Joshi, *Colloid Polym. Sci.*, 2016, **294**, 207–213.
121. D. A. Giljohann, D. S. Seferos, W. L. Daniel, M. D. Massich, P. C. Patel and C. A. Mirkin, *Angew. Chem., Int. Ed.*, 2010, **49**, 3280–3294.
122. M. A. Hayat, *Colloidal Gold. Principles, Methods and Applications*, Academic Press, San Diego, London, 1989.
123. J. Turkevich, P. C. Stevenson and J. Hillier, *Discuss. Faraday Soc.*, 1951, **11**, 55–75.
124. J. Bonsak, J. Mayandi, A. Thøgersen, E. S. Marstein and U. Mahalingam, *Phys. Status Solidi C*, 2011, **8**, 924–927.
125. J. W. Guo, T. S. Zhao, J. Prabhuram and C. W. Wong, *Electrochim. Acta*, 2005, **50**, 1973–1983.
126. S. Sali, H. R. Mackey and A. A. Abdala, *Nanomaterials*, 2019, **9**, 769.
127. S. Pei and H. M. Cheng, *Carbon N. Y.*, 2012, **50**, 3210–3228.
128. B. C. Brodie, *R. Soc. London*, 1858, **149**, 423–429.
129. W. S. Hummers and R. E. Offeman, *J. Am. Chem. Soc.*, 1958, **80**, 1339.
130. M. H. Naveen, H. B. Noh, M. S. Al Hossain, J. H. Kim and Y.-B. Shim, *J. Mater. Chem. A*, 2015, **3**, 5426–5433.
131. D. C. Marcano, D. V. Kosynkin, J. M. Berlin, A. Sinitskii, Z. Sun, A. Slesarev, L. B. Alemany, W. Lu and J. M. Tour, *ACS Nano*, 2010, **4**, 4806–4814.
132. P. P. Brisebois and M. Sijaj, *J. Mater. Chem. C*, 2020, **8**, 1517–1547.

133. X. Ruan, D. Liu, X. Niu, Y. Wang, C. D. Simpson, N. Cheng, D. Du and Y. Lin, *Anal. Chem.*, 2019, **91**, 13847–13854.
134. D. Tasis, N. Tagmatarchis, A. Bianco and M. Prato, *Chem. Rev.* 2006, **106**, 1105–1136.
135. V. Schroeder, S. Savagatrup, M. He, S. Lin and T. M. Swager, *Chem. Rev.* 2019, **119**, 599–663.
136. Y. Huang, J. Ren and X. Qu, *Chem. Rev.* 2019, **119**, 4357–4412.
137. H. Wang, P. H. Li, D. Q. Yu, Y. Zhang, Z. Z. Wang, C. Q. Liu, H. Qiu, Z. Liu, J. S. Ren and X. G. Qu, *Nano Lett.* 2018, **18**, 3344–3351.
138. H Wang, H. Jiang, S. Wang, W. B. Shi, J. C. He, H. Liu and Y. M. Huang, *RSC Adv.* 2014, **4**, 45809–45815.
139. A. Hayat, W. Haider, Y. Raza and J. L. Marty, *Talanta* 2015, **143**, 157–161.
140. H. Wang, S. Li, Y. M. Si, Z. Z. Sun, S. Y. Li and Y. H. Lin, *J. Mater. Chem. B* 2014, **2**, 4442–4448.
141. J. Qian, X. W. Yang, Z. T. Yang, G. B. Zhu, H. P. Mao and K. Wang, *J. Mater. Chem. B* 2015, **3**, 1624–1632.
142. Y. F. Zhang, C. L. Xu and B. X. Li, *RSC Adv.* 2013, **3**, 6044–6050.
143. Y. Lv, M. Ma, Y. Huang and Y. Xia, *Chem. Eur. J.* 2019, **25**, 954–960.
144. H. Li, Z. Kang, Y. Liu and S. T. Lee, *J. Mater. Chem.*, 2012, **22**, 24230–24253.
145. X. Wang, Y. Feng, P. Dong and J. Huang, *Front. Chem.*, 2019, **7**, Article 671.
146. K. Nekoueian, M. Amiri, M. Sillanpää, F. Marken, R. Boukherroub and S. Szunerits, *Chem. Soc. Rev.*, 2019, **48**, 4281–4316
147. S. Y. Lim, W. Shen and Z. Gao, *Chem. Soc. Rev.*, 2015, **44**, 362–381.
148. M. Shamsipur, A. Safavi, Z. Mohammadpour, *Sens. Actuators B Chem.* 2014, **199**, 463–469.
149. W. Shi, Q. Wang, Y. Long, Z. Cheng, S. Chen, H. Zheng, Y. Huang, *Chem. Commun.* 2011, **47**, 6695–6697.
150. Z. Mohammadpour, A. Safavi, M. Shamsipur, *Chem. Eng. J.* 2014, **255**, 1–7
151. C. Li, Y. Yang, D. Wu, T. Li, Y. Yin and G. Li, *Chem. Sci.*, 2016, **7**, 3011–3016.
152. Y. Hu, X. J. Gao, Y. Zhu, F. Muhammad, S. Tan, W. Cao, S. Lin, Z. Jin, X. Gao and H. Wei, *Chem. Mater.*, 2018, **30**, 6431–6439.
153. C. N. Loynachan, M. R. Thomas, E. R. Gray, D. A. Richards, J. Kim, B. S. Miller, J. C. Brookes, S. Agarwal, V. Chudasama, R. A. McKendry and M. M. Stevens, *ACS Nano*, 2018, **12**, 279–288.
154. C. J. Yu, C. Y. Lin, C. H. Liu, T. L. Cheng and W. L. Tseng, *Biosens. Bioelectron.*, 2010, **26**, 913–917.
155. M. Il Kim, J. Shim, T. Li, J. Lee and H. G. Park, *Chem. - A Eur. J.*, 2011, **17**, 10700–10707.
156. Y. L. Dong, H. G. Zhang, Z. U. Rahman, L. Su, X. J. Chen, J. Hu and X. G. Chen, *Nanoscale*, 2012, **4**, 3969–3976.
157. F. Huang, J. Wang, W. Chen, Y. Wan, X. Wang, N. Cai, J. Liu and F. Yu, *J. Taiwan Inst. Chem. Eng.*, 2018, **83**, 40–49.
158. M. K. Masud, J. Kim, M. M. Billah, K. Wood, M. J. A. Shiddiky, N.-T. Nguyen, R. K. Parsapur, Y. V. Kaneti, A. A. Alshehri, Y. G. Alghamidi, K. A. Alzahrani, M. Adharvanachari, P. Selvam, M. S. A. Hossain and Y. Yamauchi, *J. Mater. Chem. B*, 2019, **7**, 5412–5422.



159. X. Wang, W. Cao, L. Qin, T. Lin, W. Chen, S. Lin, J. Yao, X. Zhao, M. Zhou, C. Hang and H. Wei, *Theranostics*, 2017, **7**, 2277–2286.
160. X. Wang, X. J. Gao, L. Qin, C. Wang, L. Song, Y. N. Zhou, G. Zhu, W. Cao, S. Lin, L. Zhou, K. Wang, H. Zhang, Z. Jin, P. Wang, X. Gao and H. Wei, *Nat. Commun.*, 2019, **10**, 1–8.
161. T. Hossain, G. Mahmudunnabi, M. K. Masud, M. N. Islam, L. Ooi, K. Konstantinov, M. S. Al Hossain, B. Martinac, G. Alici, N.-T. Nguyen and M. J. A. Shiddiky, *Biosens. Bioelectron.*, 2017, **94**, 63–73.
162. J. Shah, R. Purohit, R. Singh, A. S. Karakoti and S. Singh, *J. Colloid Interface Sci.*, 2015, **456**, 100–107.
163. N. De Acha, C. Elosúa, J. M. Corres and F. J. Arregui, *Sensors (Switzerland)*, 2019, **19**, 599.
164. R. Zhang, S. He, C. Zhang and W. Chen, *J. Mater. Chem. B*, 2015, **3**, 4146–4154.
165. M. H. Lee, J. S. Kim and J. L. Sessler, *Chem. Soc. Rev.*, 2015, **44**, 4185–4191.
166. W. Deng, Y. Peng, H. Yang, Y. Tan, M. Ma, Q. Xie and S. Chen, *ACS Appl. Mater. Interfaces*, 2019, **11**, 29072–29077.
167. M. H. Naveen, N. G. Gurudatt and Y.-B. Shim, *Appl. Mater. Today*, 2017, **9**, 419–433.
168. E. O. Blair and D. K. Corrigan, *Biosens. Bioelectron.*, 2019, **134**, 57–67.
169. N. Soda, B. H. A. Rehm, P. Sonar, N.-T. Nguyen and M. J. A. Shiddiky, *J. Mater. Chem. B*, 2019, **7**, 6670–6704.
170. M. K. Masud, J. Na, M. Younus, M. S. A. Hossain, Y. Bando, M. J. A. Shiddiky and Y. Yamauchi, *Chem. Soc. Rev.*, 2019, **48**, 5717–5751.
171. K. M. Koo, L. G. Carrascosa, M. J. A. Shiddiky and M. *Anal. Chem.*, 2016, **88**, 2000–2005.
172. M. N. Islam, M. K. Masud, M. H. Haque, M. S. A. Hossain, Y. Yamauchi, N.-T. Nguyen and M. J. A. Shiddiky, *Small Methods*, 2017, **1**, 1700131.
173. J. Wang, J. Chen and S. Sen, *J. Cell. Physiol.*, 2016, **231**, 25–30.
174. M. N. Islam, L. Gorgannezhad, M. K. Masud, S. Tanaka, M. S. A. Hossain, Y. Yamauchi, N.-T. Nguyen and M. J. A. Shiddiky, *ChemElectroChem*, 2018, **5**, 2488–2495.
175. K. Boriachek, M. Umer, M. N. Islam, V. Gopalan, A. K. Lam, N.-T. Nguyen and M. J. A. Shiddiky, *Analyst*, 2018, **143**, 1662–1669.
176. M. Kamal Masud, M. N. Islam, M. H. Haque, S. Tanaka, V. Gopalan, G. Alici, N.-T. Nguyen, A. K. Lam, M. S. A. Hossain, Y. Yamauchi and M. J. A. Shiddiky, *Chem. Commun.*, 2017, **53**, 8231–8234.
177. M. N. Islam, M. K. Masud, N.-T. Nguyen, V. Gopalan, H. R. Alamri, Z. A. Alothman, M. S. A. Hossain, Y. Yamauchi, A. K. Y. Lam and M. J. A. Shiddiky, *Biosens. Bioelectron.*, 2018, **101**, 275–281.
178. M. N. Islam, M. K. Masud, M. H. Haque, M. S. A. Hossain, Y. Yamauchi, N.-T. Nguyen and M. J. A. Shiddiky, *Small Methods*, 2017, **1**, 1700131.
179. M. Umer, R. Vaidyanathan, N. T. Nguyen and M. J. A. Shiddiky, *Biotechnol. Adv.*, 2018, **36**, 1367–1389.
180. F. S. Felix and L. Angnes, *Biosens. Bioelectron.*, 2018, **102**, 470–478.
181. Y. Li, Y. Zhang, F. Li, J. Feng, M. Li, L. Chen and Y. Dong, *Biosens. Bioelectron.*, 2017, **92**, 33–39.

182. F. Li, Y. Li, J. Feng, Z. Gao, H. Lv, X. Ren and Q. Wei, *Biosens. Bioelectron.*, 2018, **100**, 512–518.
183. L. Zhang, X. Xie, Y. Yuan, Y. Chai and R. Yuan, *Electroanalysis*, 2019, **31**, 1019–1025.
184. M. Jarczewska, Ł. Górski and E. Malinowska, *Anal. Methods*, 2016, **8**, 3861–3877.
185. Y. Zhu, P. Chandra, K. M. Song, C. Ban and Y. B. Shim, *Biosens. Bioelectron.*, 2012, **36**, 29–34.
186. X. Wang, L. Cohen, J. Wang and D. R. Walt, *J. Am. Chem. Soc.*, 2018, **140**, 18132–18139.
187. W. Wang, L. Liu, L. Xu, H. Kuang, J. Zhu and C. Xu, *Part. Part. Syst. Charact.*, 2016, **33**, 388–395.
188. C. Wang, C. Liu, J. Luo, Y. Tian and N. Zhou, *Anal. Chim. Acta*, 2016, **936**, 75–82.
189. D. S. Wishart, *PLoS Comput. Biol.*, 2012, **8**, e1002805.
190. K. J. Cash and H. A. Clark, *Trends Mol. Med.*, 2010, **16**, 584–593.
191. K. Rathee, V. Dhull, R. Dhull and S. Singh, *Biochem. Biophys. Reports*, 2016, **5**, 35–54.
192. J. Bakker, P. Gris, M. Coffernils, R. J. Kahn and J. L. Vincent, *Am. J. Surg.*, 1996, **171**, 221–226.
193. N. P. Sardesai, M. Ganesana, A. Karimi, J. C. Leiter and S. Andreescu, *Anal. Chem.*, 2015, **87**, 2996–3003.
194. S. Tanaka, Y. V. Kaneti, R. Bhattacharjee, M. N. Islam, R. Nakahata, N. Abdullah, S. I. Yusa, N.-T. Nguyen, M. J. A. Shiddiky, Y. Yamauchi and M. S. A. Hossain, *ACS Appl. Mater. Interfaces*, 2018, **10**, 1039–1049.
195. E. V. Karpova, E. V. Shcherbacheva, A. A. Galushin, D. V. Vokhmyanina, E. E. Karyakina and A. A. Karyakin, *Anal. Chem.*, 2019, **91**, 3778–3783.
196. J. Zhu, X. Peng, W. Nie, Y. Wang, J. Gao, W. Wen, J. N. Selvaraj, X. Zhang and S. Wang, *Biosens. Bioelectron.*, 2019, **141**, 111450.
197. M. Wu, S. Meng, Q. Wang, W. Si, W. Huang and X. Dong, *ACS Appl. Mater. Interfaces*, 2015, **7**, 21089–21094.
198. D. V. Vokhmyanina, K. D. Andreeva, M. A. Komkova, E. E. Karyakina and A. A. Karyakin, *Talanta*, 2020, **208**, 120393.
199. E. V. Karpova, A. I. Laptev, E. A. Andreev, E. E. Karyakina and A. A. Karyakin, *ChemElectroChem*, 2020, **7**, 191–194.
200. K. Wang, C. Wu, F. Wang, M. Liao and G. Jiang, *Biosens. Bioelectron.*, 2020, **150**, 111869.
201. S. H. Wen, X. L. Zhong, Y. Di Wu, R. P. Liang, L. Zhang and J. D. Qiu, *Anal. Chem.*, 2019, **91**, 6487–6497.
202. F. Xiao, L. Wang and H. Duan, *Biotechnol. Adv.*, 2016, **34**, 234–249.
203. Z. Da Gao, Y. Qu, T. Li, N. K. Shrestha and Y. Y. Song, *Sci. Rep.*, 2014, **4**, 6891.
204. M. A. Komkova, E. E. Karyakina and A. A. Karyakin, *J. Am. Chem. Soc.*, 2018, **140**, 11302–11307.
205. G. M. Whitesides, *Nature*, 2006, **442**, 368–73.
206. H. Moghadas, M. S. Saidi, N. Kashaninejad and N.-T. Nguyen, *Drug Deliv. Transl. Res.*, 2018, **8**, 830–842.

207. N. Kashaninejad, M. J. A. Shiddiky and N.-T. Nguyen, *Adv. Biosyst.*, 2018, **2**, 1700197.
208. R. Vadivelu, N. Kashaninejad, K. R. Sreejith, R. Bhattacharjee, I. Cock and N.-T. Nguyen, *ACS Appl. Mater. Interfaces*, 2018, **10**, 43439–43449.
209. N. Kashaninejad, M. Yaghoobi, M. Pourhassan-Moghaddam, S. R. Bazaz, D. Jin and M. E. Warkiani, *Nanotechnol. Microfluid.*, 2020, 211–238.
210. G.-P. Nikoleli, C. G. Siontorou, D. P. Nikolelis, S. Bratakou, S. Karapetis and N. Tzamtzis, in *Nanotechnology and Biosensors*, eds. D. P. Nikolelis and G.-P. Nikoleli, Elsevier, 2018, pp. 375–394.
211. Y. Song, Y. Zhang, P. E. Bernard, J. M. Reuben, N. T. Ueno, R. B. Arlinghaus, Y. Zu and L. Qin, *Nat. Commun.*, 2012, **3**, 1283.
212. Y. Song, X. Xia, X. Wu, P. Wang and L. Qin, *Angew. Chem., Int. Ed.*, 2014, **53**, 12451–12455.
213. Z. Zhu, Z. Guan, S. Jia, Z. Lei, S. Lin, H. Zhang, Y. Ma, Z.-Q. Tian and C. J. Yang, *Angew. Chem., Int. Ed.*, 2014, **53**, 12503–12507.
214. I. Ortiz-Gómez, A. Salinas-Castillo, A. G. García, J. A. Álvarez-Bermejo, I. de Orbe-Payá, A. Rodríguez-Diéguez and L. F. Capitán-Vallvey, *Microchim. Acta*, 2017, **185**, 47.
215. P. Zhang, D. Sun, A. Cho, S. Weon, S. Lee, J. Lee, J. W. Han, D.-P. Kim and W. Choi, *Nat. Commun.*, 2019, **10**, 940.
216. H. Cheng, L. Zhang, J. He, W. Guo, Z. Zhou, X. Zhang, S. Nie and H. Wei, *Anal. Chem.*, 2016, **88**, 5489–5497.
217. R. Shen, P. Liu, Y. Zhang, Z. Yu, X. Chen, L. Zhou, B. Nie, A. Żaczek, J. Chen and J. Liu, *Anal. Chem.*, 2018, **90**, 4478–4484.
218. K. M. Koo, S. Dey and M. Trau, *ACS Sensors*, 2018, **3**, 2597–2603.
219. E. Ko, V.-K. Tran, S. E. Son, W. Hur, H. Choi and G. H. Seong, *Sensors Actuators B Chem.*, 2019, **294**, 166–176.
220. Z. Zhang, Y. Li, X. Zhang and J. Liu, *Nanoscale*, 2019, **11**, 4854–4863.
221. X. Lian, Y. Fang, E. Joseph, Q. Wang, J. Li, S. Banerjee, C. Lollar, X. Wang and H.-C. Zhou, *Chem. Soc. Rev.*, 2017, **46**, 3386–3401.
222. N. Liu, Z. Xu, A. Morrin and X. Luo, *Anal. Methods*, 2019, **11**, 702–711.
223. N.-T. Nguyen, M. Hejazian, C. H. Ooi and N. Kashaninejad, *Micromachines*, 2017, **8**, 186.
224. P. Rostami, N. Kashaninejad, K. Moshksayan, M. S. Saidi, B. Firoozabadi and N.-T. Nguyen, *J. Sci. Adv. Mater. Devices*, 2019, **4**, 1–18.
225. S. Yadav, N. Kashaninejad, M. K. Masud, Y. Yamauchi, N.-T. Nguyen and M. J. A. Shiddiky, *Biosens. Bioelectron.*, 2019, **139**, 111315.

## Figure Captions

**Figure 1.** Schematic presentation of the typical enzyme-mimetic activities of nanozymes, their advantages, and limitations compared to natural enzymes, recommended strategies to improve their substrate specificity, and their applications in electrochemical biosensors.

**Figure 2.** Classification of nanozymes.<sup>4,48,49</sup> (\*) Mark represents the nanozymes commonly used for electrochemical biosensors.

**Figure 3.** (a) Schematic representation of paper based lateral flow immunoassays (LIFA). Antibody functionalized Pt nanocatalysts (PtNCs) and biotinylated nanobody fragments are mixed with the test samples (*i.e.*, plasma or serum). If the test samples contain target p24 capsid protein, it sandwiched between the antibody–PtNC and biotinylated nanobody fragment, forming a biotinylated complex. A lateral flow strip, composed of a nitrocellulose reaction membrane and an absorbent pad, is used to draw this complex up the strip toward a streptavidin-modified test line by capillary action. At the test line, the peroxidase-like activity of PtNCs is used to catalyze the oxidation of CN/DAB substrate in the presence of H<sub>2</sub>O<sub>2</sub> producing an insoluble black product (*i.e.*, naked-eye observation). (b) Site-selective chemical modification of a nanobody with an exposed cysteine mutation (red), where lysine residues are highlighted in orange on the structural model (left), and cartoon of oriented elements at the streptavidin test line. (c) Comparison of dynamic ranges of 4<sup>th</sup> generation LIFA, ELISA and PtNC LIFA.

Reprinted with permission from Ref (154)

(<https://pubs.acs.org/doi/abs/10.1021/acsnano.7b06229>). Copyright (2018) American Chemical Society. Further permissions related to the material excerpted should be directed to the American Chemical Society.

**Figure 4.** Schematic representation of the nanozyme's catalytic activities and its application in the electrochemical biosensor. Nanozymes can be functionalized with a range of receptor probes (e.g., complementary capture probes for DNA and RNA targets, antibodies for proteins, etc.) by conventional surface modification procedures. The probe-functionalized nanozymes can capture the targets (e.g., pathogen, cancer cell, exosome, nucleic acid) via the specific interaction between nanozyme-bound probes and targets. The nanozymes-attached targets can then be quantified electrochemically or optically (i.e., naked eye and UV-visible) via an ELISA-type sandwich immunoassay or sandwich hybridization method.

**Figure 5.** (A) Synthesis of FeTCPP@MOF nanozymes followed by covalent coupling with streptavidin (SA) to form FeTCPP@MOF-SA composite and (B) Target binding initiates allosteric switch of the hairpin probe allows FeTCPP@MOF-SA to recognize the probe and o-PD oxidation provides the electrochemical signal. Reprinted with permission from Ref. (69) (<https://doi.org/10.1021/acs.analchem.5b00001>). Copyright (2015) American Chemical Society.

**Figure 6.** Schematic representation of naked eye and electrochemical detection of p53 autoantibody where target recognition and electrochemical measurement are operated in two separated electrodes. Reprinted with permission from Ref. (54) (<https://doi.org/10.1021/acs.analchem.5b00001>). Copyright (2017) American Chemical Society.

**Figure 7.** Schematic representation of layer-by-layer (LBL) assembly of the nonenzymatic nanoprobe NP1 (aptamer) and NP2 (cDNA) and NTH-assisted dual-aptamer based electrochemical sensor for detection of cTnI. Reprinted from Ref. (75) (<https://doi.org/10.1016/j.bios.2019.03.049>), Scheme 1, Copyright (2019), with permission from Elsevier.

**Table**

**Table 1: Nanozymes used in electrochemical sensors for biomarker detection**

Nanozyme	Function	Substrate	Target	LOD	Ref.
CoFe <sub>2</sub> O <sub>4</sub> MNPs	Nano electrocatalyst for toluidine blue catalysis	Toluidine blue	microRNA (i.e., microRNA-21)	0.3 fM	66
PdNPs@Fe-MOFs	Tracer indicator	TMB + H <sub>2</sub> O <sub>2</sub>	microRNA (i.e., microR-122)	0.003 fM	67
Fe <sub>3</sub> O <sub>4</sub> and Cu(II) complex	Fe <sub>3</sub> O <sub>4</sub> NPs acts as a magnetic nanocarrier Increase of sensitivity because of the synergistic effect of Fe <sub>3</sub> O <sub>4</sub> nanozyme and Cu(II) complex.	TMB + H <sub>2</sub> O <sub>2</sub>	microRNA (microR-21)	33 aM	68
FeTCPP@MOF composites	Increased diffusion of <i>o</i> -PD permitted by the porous structure of nanozyme	<i>o</i> -PD + H <sub>2</sub> O <sub>2</sub>	DNA	0.48 fM	69
Au@PtNPs	Used as a trace tag	PNP + NaBH <sub>4</sub>	DNA	0.3aM	70
ZrHCF MNPs	DNA can be bound to ZrHCF MNPs through the interaction from phosphate group from DNA and Zr(IV) from ZrHCF without chemical modification.	H <sub>2</sub> O <sub>2</sub>	DNA	0.43 fM	71
hemin/G-quadruplex DNAzyme	-	TMB + H <sub>2</sub> O <sub>2</sub>	HBV DNA	0.5 pM	72
Mesoporous Iron Oxide (MIO)	MIO functionalized with 5mC antibody recognizes 5mC immobilized on SPGE	TMB + H <sub>2</sub> O <sub>2</sub>	Global DNA methylation (5mC)	10% of methylation in genomic DNA	53

Au@NPFe <sub>2</sub> O <sub>3</sub> NC	Nanocarriers for target p53 from serum	TMB + H <sub>2</sub> O <sub>2</sub>	p53 autoantibodies	0.02 U mL <sup>-1</sup>	73
Au-NPFe <sub>2</sub> O <sub>3</sub> NC	Direct isolation of target protein from serum	TMB + H <sub>2</sub> O <sub>2</sub>	p53 autoantibody	0.08 U mL <sup>-1</sup>	54
Fe <sub>3</sub> O <sub>4</sub> /Au@Pt	Used as a nanocarrier for natural HRP, DNAzymes and aptamer.  Co-catalysis for signal enhancement	Hydroquinone (HQ) + H <sub>2</sub> O <sub>2</sub>	Cardiac troponin (cTnI)	7.5 pg mL <sup>-1</sup>	74
Fe <sub>3</sub> O <sub>4</sub> @UiO-66/Cu@Au	Formation of cluster-based nanoprobe for further enhancing detection sensitivity	HQ + H <sub>2</sub> O <sub>2</sub>	Cardiac troponin (cTnI)	16 pg mL <sup>-1</sup>	75
Mn <sub>3</sub> O <sub>4</sub> /Pd@Pt	Used for nanoprobe formation which will increase further sensitivity through loaded with HRP.	HQ + H <sub>2</sub> O <sub>2</sub>	HER2	0.08 ng mL <sup>-1</sup>	76
Pt-Cu HTBNFs	Bind to target through anchored detection antibody and act as a signal enhancer.	H <sub>2</sub> O <sub>2</sub>	PSA	0.03 pg mL <sup>-1</sup>	77
Au@ZIF-8(NiPd)	Thrombin binding aptamer anchored Au@ZIF-8(NiPd) act as a signaling probe.	H <sub>2</sub> O <sub>2</sub>	Thrombin (TB)	15 fM	78
Au@MGN (gold-magnetic graphene nanocomposite)	Antibody functionalized Au@MGN forms sandwich	H <sub>2</sub> O <sub>2</sub>	Tissue polypeptide antigen	7.5 fg mL <sup>-1</sup>	79
Pt@P-MOF(Fe)	Catalyst and redox mediator to detect telomerase activity.	H <sub>2</sub> O <sub>2</sub>	Telomerase activity	Telomerase activity form 20 HeLa cells	80

				per mL	
Au-NPFe <sub>2</sub> O <sub>3</sub> NC	Tetraspanin functionalized nanocubes were used as a dispersible capture agent for bulk exosome	TMB + H <sub>2</sub> O <sub>2</sub>	Exosome	10 <sup>3</sup> exosomes per mL	55
CuO/WO <sub>3</sub> -GO	Folic acid-modified CuO/WO <sub>3</sub> -GO capture cancer cell by recognizing folate receptor results in signal attenuation.	OPD+H <sub>2</sub> O <sub>2</sub>	Cancer cells	18 cells per mL	29
NGQD@NC@Pd HNS	Electrocatalytic reduction of H <sub>2</sub> O <sub>2</sub> released by cancer cells.	H <sub>2</sub> O <sub>2</sub>	Cancer cells	-	81
CuO	MUC-1 aptamer modified CuO nanozyme was used for selective binding to MCF-7 CTCs and catalyzing the reduction of H <sub>2</sub> O <sub>2</sub> for higher sensitivity	H <sub>2</sub> O <sub>2</sub>	CTCs	27 cells per mL	58
rGO/MoS <sub>2</sub> composites with Fe <sub>3</sub> O <sub>4</sub> NPs bienzyme	Immunomagnetic beads (Fe <sub>3</sub> O <sub>4</sub> NPs) help in the enrichment of CTCs.  Synergistic peroxidase activity of rGO/MoS <sub>2</sub> and Fe <sub>3</sub> O <sub>4</sub> NPs for signal amplification	TMB + H <sub>2</sub> O <sub>2</sub>	CTCs	6 cells per mL	82
Graphene Quantum Dots (GQD)	-	H <sub>2</sub> O <sub>2</sub>	<i>Yersinia enterocolitica</i>	5 CFU/mL (milk) 30 CFU/mL	83



				(human serum)	
Gold nanoparticles (GNPs)	F23 aptamer leaves GNPs after interacting with <i>Pseudomonas aeruginosa</i> which ensures the revive of peroxidase activity of GNPs	TMB	<i>Pseudomonas aeruginosa</i>	60 CFU/mL	50
Co <sub>3</sub> (PO <sub>4</sub> ) <sub>2</sub> NRs	Used as electrode materials	superoxide anion (O <sub>2</sub> <sup>•-</sup> )	O <sub>2</sub> <sup>•-</sup> released from cancer cells	2.25 nM	84
Mn-MPSA-HCS And Mn-MPSA-HCC	Used as electrode materials	superoxide anion (O <sub>2</sub> <sup>•-</sup> )	O <sub>2</sub> <sup>•-</sup> released from cancer cells	1.25 nM	85
GS@ZIF-67	Used as electrode materials	Electrocatalytic Oxidation of Glucose	Glucose	0.36 μM	86
Poly Acrylic Acid-Coated Nanoceria(PNC)	PNC catalyse TMB in the absence H <sub>2</sub> O <sub>2</sub>	TMB	Norepinephrine	66 nM	87
h-CuS NCs	-	TMB+H <sub>2</sub> O <sub>2</sub>	Glucose	-	88
Au/Co@HNCF	-	UA	UA	0.023 μM	89

**Figures**

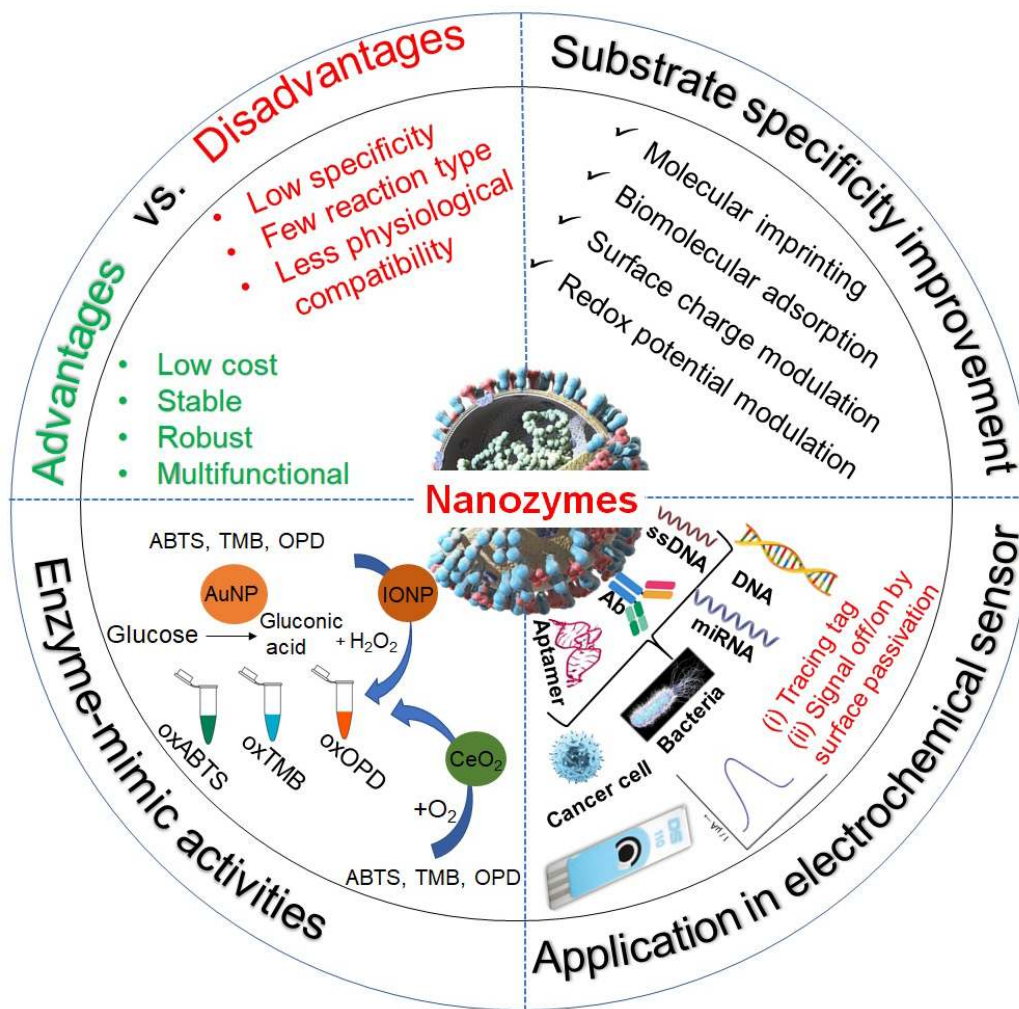


**Figure 1.**

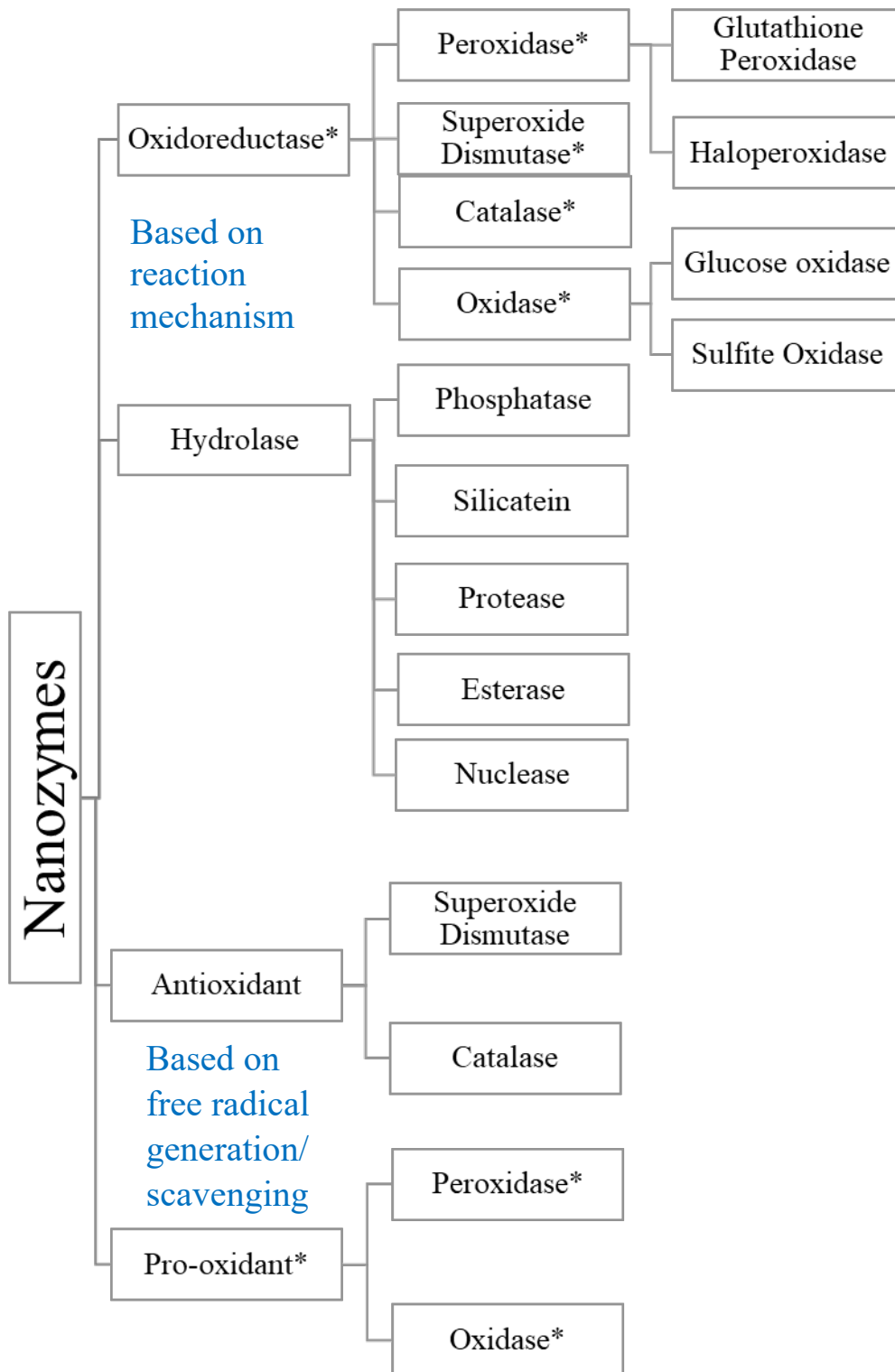


Figure 2.

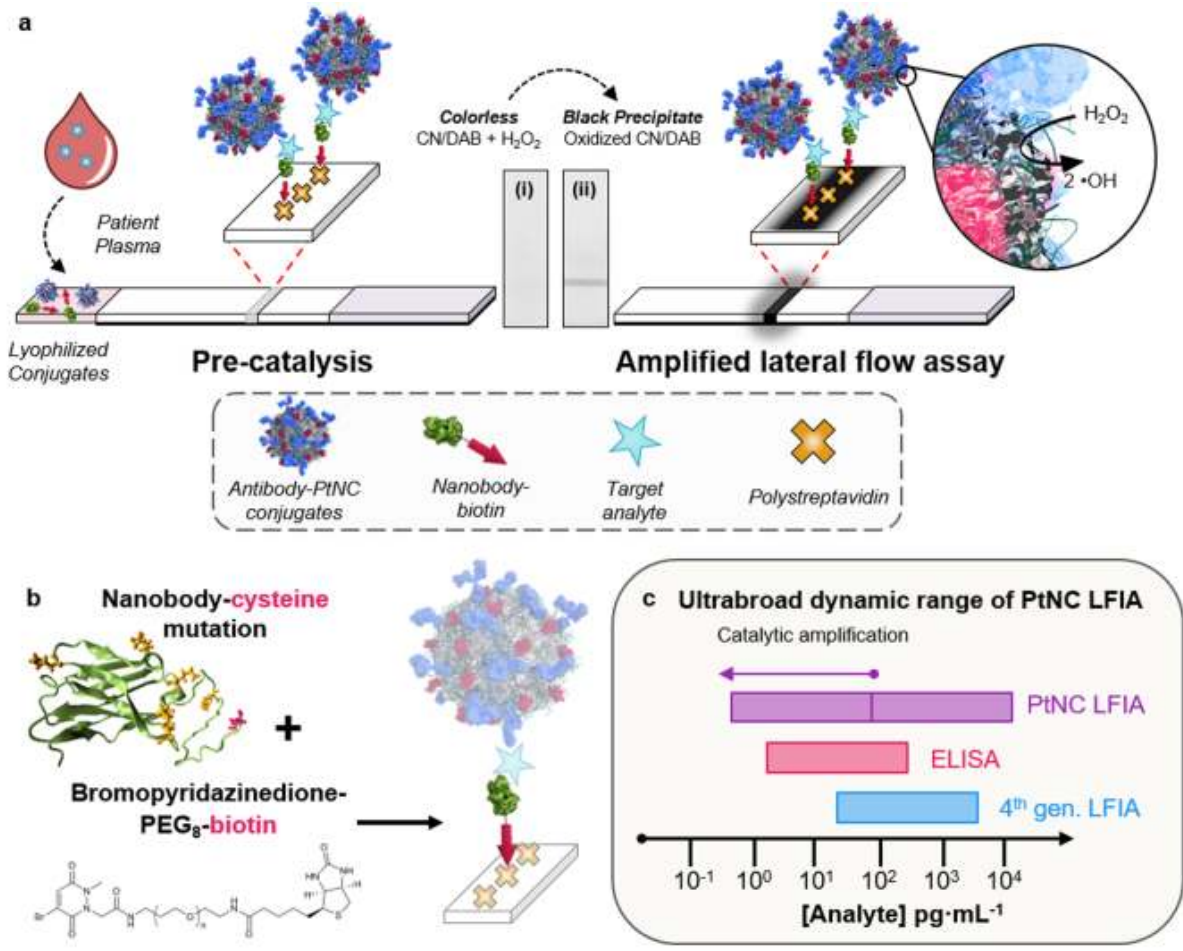


Figure 3

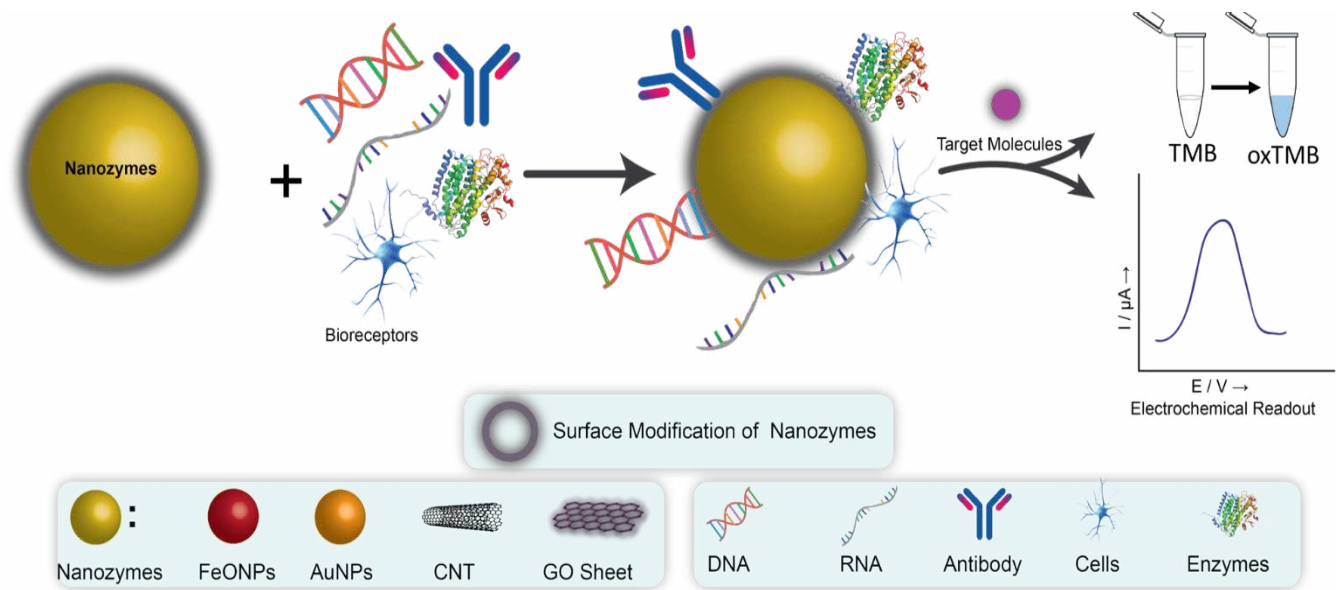


Figure 4

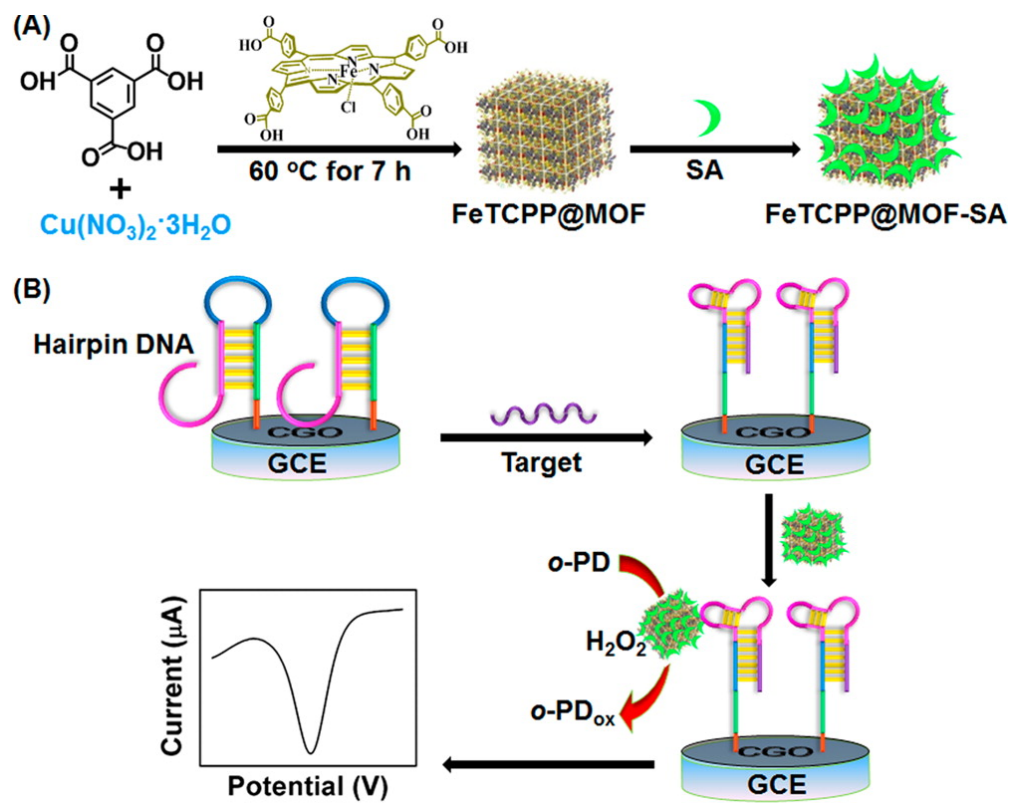


Figure 5

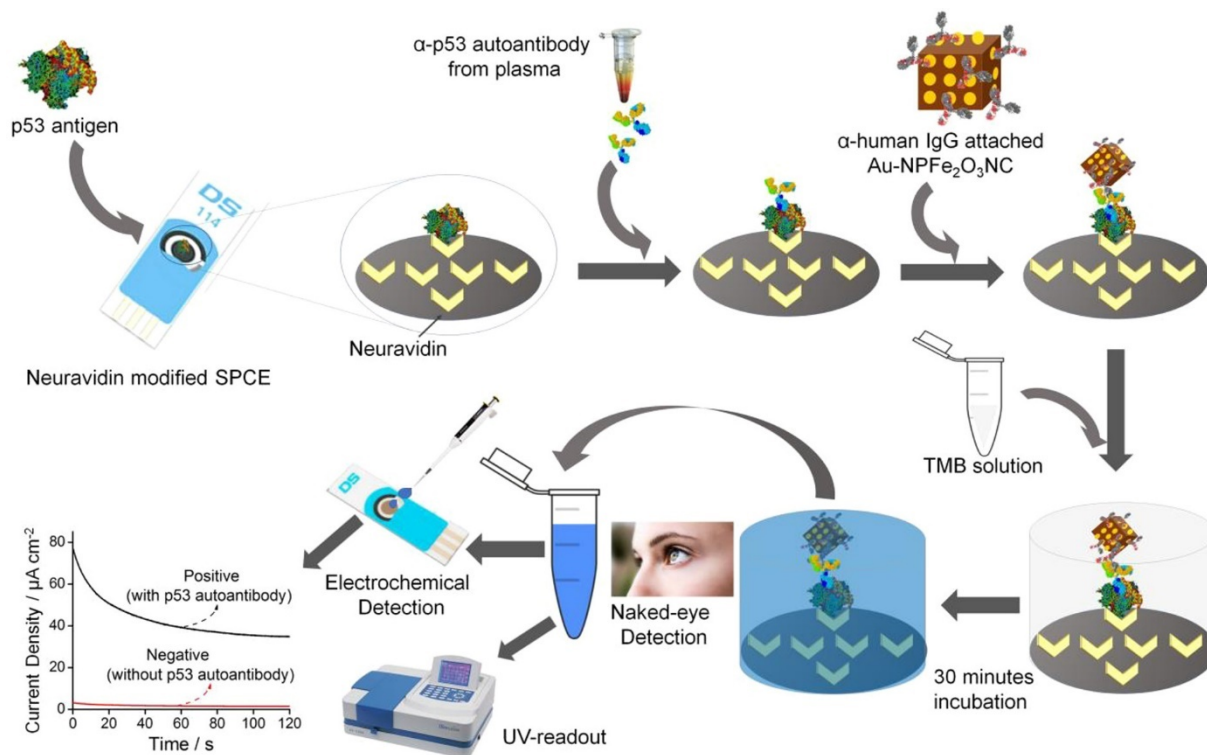


Figure 6

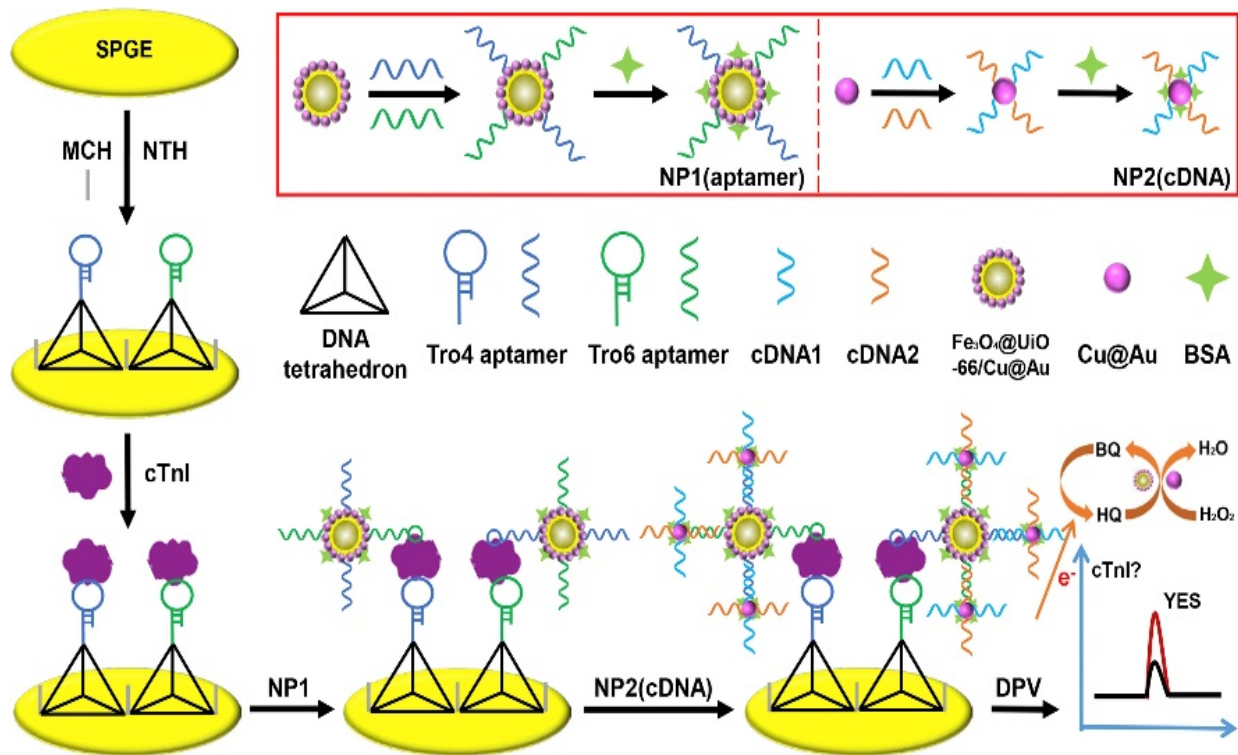


Figure 7